REPORT DOCUMENTATION PAGE

1. REPORT DATE (DD-MM-YYYY)	2. REPORT TYPE	3. DATES COVERED (From - To)
09-07-2013	Final Report	1-May-2010 - 30-Nov-2013

4. TITLE AND SUBTITLE	5a. CONTRACT NUMBER
Vertically Oriented Graphene Electrochemical Double Layer Capacitor with Very Fast Dynamic Response	W911NF-10-1-0121
	5b. GRANT NUMBER
	5c. PROGRAM ELEMENT NUMBER
	0620BE

6. AUTHORS	5d. PROJECT NUMBER
Ronald A. Outlaw	
	5e. TASK NUMBER
	5f. WORK UNIT NUMBER

7. PERFORMING ORGANIZATION NAMES AND ADDRESSES	8. PERFORMING ORGANIZATION REPORT NUMBER
College of William and Mary Office of Research and Grants P.O. Box 8795 Williamsburg, VA 23187 -8795	

9. SPONSORING/MONITORING AGENCY NAME(S) AND ADDRESS(ES)	10. SPONSOR/MONITOR'S ACRONYM(S)
U.S. Army Research Office P.O. Box 12211 Research Triangle Park, NC 27709-2211	ARO
	11. SPONSOR/MONITOR'S REPORT NUMBER(S)
	58116-CH-DRP.3

12. DISTRIBUTION AVAILIBILITY STATEMENT

Approved for Public Release; Distribution Unlimited

13. SUPPLEMENTARY NOTES

The views, opinions and/or findings contained in this report are those of the author(s) and should not contrued as an official Department of the Army position, policy or decision, unless so designated by other documentation.

14. ABSTRACT

Activated carbon materials are expected to play a crucial role in supercapacitor technology. To date, they are the most preferred choice because they can be processed to have exceptionally high surface area, relatively high electric conductivity and are reasonably priced. This work was to improve the morphological structure of vertically oriented graphene (VOG), also called carbon nanosheets (CNS), to a higher density of taller sheets so that the total surface area is substantially increased, which increases capacitance, and more verticality to improve response time.

15. SUBJECT TERMS

electrical double layer capacitors, vertically oriented graphene nanosheets

16. SECURITY CLASSIFICATION OF:			17. LIMITATION OF ABSTRACT	15. NUMBER OF PAGES	19a. NAME OF RESPONSIBLE PERSON
a. REPORT	b. ABSTRACT	c. THIS PAGE			Ronald Outlaw
UU	UU	UU	UU		19b. TELEPHONE NUMBER 757-221-7735

Vertically Oriented Graphene Electrochemical Double Layer Capacitor with Very Fast Dynamic Response

ABSTRACT

Activated carbon materials are expected to play a crucial role in supercapacitor technology. To date, they are the most preferred choice because they can be processed to have exceptionally high surface area, relatively high electric conductivity and are reasonably priced. This work was to improve the morphological structure of vertically oriented graphene (VOG), also called carbon nanosheets (CNS), to a higher density of taller sheets so that the total surface area is substantially increased, which increases capacitance, and more verticality to improve response time. An increase in the surface area of a factor of four resulted in only a factor of two increase in capacitance. Parametric studies in radio frequency plasma enhanced chemical vapor deposition (RF PECVD) growth and the use of gridded mesh on the substrate with a bias voltage provided higher density growth of the vertically oriented graphitic sheets. It was anticipated that, eventually, there would be a sheet density and sheet height that substantially impacts the dynamic response because of decreasing electrolyte conductance, but that was not yet observed.

Enter List of papers submitted or published that acknowledge ARO support from the start of the project to the date of this printing. List the papers, including journal references, in the following categories:

<div align="center">

(a) Papers published in peer-reviewed journals (N/A for none)

</div>

<u>Received</u>   <u>Paper</u>

  TOTAL:

Number of Papers published in peer-reviewed journals:

<div align="center">

(b) Papers published in non-peer-reviewed journals (N/A for none)

</div>

<u>Received</u>   <u>Paper</u>

  TOTAL:

Number of Papers published in non peer-reviewed journals:

<div align="center">

(c) Presentations

</div>

Number of Presentations: 0.00

<div align="center">

Non Peer-Reviewed Conference Proceeding publications (other than abstracts):

</div>

Received   Paper

TOTAL:

Number of Non Peer-Reviewed Conference Proceeding publications (other than abstracts):

Peer-Reviewed Conference Proceeding publications (other than abstracts):

Received   Paper

TOTAL:

Number of Peer-Reviewed Conference Proceeding publications (other than abstracts):

(d) Manuscripts

Received   Paper

08/17/2011   2.00   . Graphene EDL capacitor with ultrahigh power performance,
                     Electrochimica Acta (08 2011)

TOTAL: **1**

Number of Manuscripts:

Books

Received   Paper

TOTAL:

Patents Submitted

Patents Awarded

Awards

Graduate Students

NAME	PERCENT_SUPPORTED
FTE Equivalent:	
Total Number:	

Names of Post Doctorates

NAME	PERCENT_SUPPORTED
FTE Equivalent:	
Total Number:	

Names of Faculty Supported

NAME	PERCENT_SUPPORTED	National Academy Member
Ronald A. Outlaw	1.00	
FTE Equivalent:	**1.00**	
Total Number:	**1**	

Names of Under Graduate students supported

NAME	PERCENT_SUPPORTED
FTE Equivalent:	
Total Number:	

Student Metrics

This section only applies to graduating undergraduates supported by this agreement in this reporting period

The number of undergraduates funded by this agreement who graduated during this period: 0.00

The number of undergraduates funded by this agreement who graduated during this period with a degree in science, mathematics, engineering, or technology fields: 0.00

The number of undergraduates funded by your agreement who graduated during this period and will continue to pursue a graduate or Ph.D. degree in science, mathematics, engineering, or technology fields: 0.00

Number of graduating undergraduates who achieved a 3.5 GPA to 4.0 (4.0 max scale): 0.00

Number of graduating undergraduates funded by a DoD funded Center of Excellence grant for Education, Research and Engineering: 0.00

The number of undergraduates funded by your agreement who graduated during this period and intend to work for the Department of Defense 0.00

The number of undergraduates funded by your agreement who graduated during this period and will receive scholarships or fellowships for further studies in science, mathematics, engineering or technology fields: 0.00

Names of Personnel receiving masters degrees

NAME

Total Number:

Names of personnel receiving PHDs

NAME

Total Number:

Names of other research staff

NAME   PERCENT_SUPPORTED

FTE Equivalent:
Total Number:

Sub Contractors (DD882)

Inventions (DD882)

Scientific Progress

Introduction:

Activated carbon materials are expected to play a crucial role in supercapacitor technology. To date, they are the most preferred choice because they can be processed to have exceptionally high surface area, relatively high electric conductivity and are reasonably priced. This work was to improve the morphological structure of vertically oriented graphene (VOG), also called carbon nanosheets (CNS), to a higher density of taller sheets so that the total surface area is substantially increased, which increases capacitance, and more verticality to improve response time. An increase in the surface area of a factor of four resulted in only a factor of two increase in capacitance. Parametric studies in radio frequency plasma enhanced chemical vapor deposition (RF PECVD) growth and the use of gridded mesh on the substrate with a bias voltage provided higher density growth of the vertically oriented graphitic sheets. It was anticipated that, eventually, there would be a sheet density and sheet height that substantially impacts the dynamic response because of decreasing electrolyte conductance, but that was not yet observed. This optimal point that maximizes capacitance without significant loss of dynamic response is a primary growth objective. Studies to further increase the capacitance with the use of coatings, such as oxidized Mn and Ru, or the NiO-OH coated asymmetric electrode were conducted for an anticipated synergistic impact on electrical double layer capacitance (EDLC) properties, but only marginal impact was observed. Finally, edge and defects in the sheets also have been found to increase capacitance in similar structures. This suggests that (by growth, chemical alteration or by ion bombardment) an increased edge/defect density that does not significantly inhibit electron transport is an important objective. This was studied using Ar ion bombardment to increase defects.

Approach:

The following is the proposal statement of work tasks with the achievements accomplished toward completing these tasks.

Task A. Optimize capacitance of vertically oriented carbon nanosheets electrodes
Increase capacitance by maximizing the charge carrier density of the graphene.

Figure A-1. (a) Schematics of the plan and side view of the experimental setup. The Ni substrate and the stainless steel (SS) mask were grounded. (b) A schematic of the structure of vertically–oriented graphenes on Ni substrate near the base [11]. Edges are terminated with 1-3 hydrogen atoms. (c) SEM image of vertically–oriented graphenes, plan view. (d) SEM glancing incidence image showing the thickness of the vertically–oriented graphenes (e) TEM image showing a single sheet of the vertically-oriented graphenes (f) HRTEM of graphenes showing double parallel fringes (indicating by arrows) with a distance of 0.37nm at the edge. (g) AES and (h) XPS spectra of vertically-oriented graphenes showing the very high purity of the sheets.

The morphology and structure of vertically–oriented graphenes on the Ni substrate are shown in Figure A-1c and A-1d. The initial Volmer-Weber planar growth of two-dimensional graphitic islands on the Ni substrate ultimately impinge on each other, and then push the sp2 bonds upward. The dissociated carbon in the plasma then continuously provides ions and atoms to the vertically growing hexagonal lattice. The basal layer is approximately 10 nm thick. After 20-min growth, the resulting coating was comprised of vertically–oriented graphenes, ~1.5 µm high with a cross-section <1 nm thick (see Figure A-1b), having an average thickness of about one to three layers. Figure A-1e is a low magnification image showing a sheet grown vertically on the substrate. Two parallel fringes were observed from the HRTEM (Figure A-1f) at the edge of graphenes where it is bent and folded back over itself. The number of the fringes indicates that this particular sheet consist of 2 atomic layers. Most vertical sheets terminate in a single graphene sheet. The AES and XPS spectra of graphenes were shown in Figure 1g and Figure A-1f. It can be seen that, besides the C feature, only a very small amount of oxygen was detected 9 The XPS spectrum also shows predominantly C feature with a negligible amount of O due to the ambient exposure. These results indicate that the

vertically-oriented graphene sheets are virtually free of contamination (<1%). Previous temperature desorption spectroscopy does show a substantial of intercalated hydrogen [1].

When the substrate is electrically floating with the plasma, it is likely that the substrate rises to near the plasma electron/ion potential and gives a much more irregular and random morphology. However, when the substrate is grounded, an applied potential between the plasma and the films creates a local dc electric field component that more efficiently directs the movement of ions to the tallest sheets and results in a growth of graphene that is taller and has a higher sheet density compared to previous work [2, 3]. All data presented in this paper were based on the Ni substrates at 0 V.

The optical and SEM images in Figure A-2a and A-2b show the initial growth of vertical graphenes on the Ni substrate. A patch–like pattern is observed from early nucleation and growth at the grain boundary. The Ni surface away from the grain boundary is smoother and more ordered, resulting in Volmer-Weber islands forming and growing laterally until the grains impinge. This is a much slower process than that occurring at the defects of the grain boundary. The grain size of the Ni substrate determined from the optical images has a broad distribution between 10-50 μm. SEM images in Figure A-2c and A-2d show the graphenes on the boundary and the center of the grains. The graphenes along the boundary of the grains exhibit higher, thicker and more random morphology (Figure A-2c) compared to those away from the grain boundary, which are of more uniform vertical growth and thickness (Figure A-2d). Figure A-2e shows the corresponding Raman spectra of the pure Ni surface compared to the spectra of the vertical graphene on the Ni grain boundary and towards the center of the Ni grain. The Raman spectrum of the Ni substrate shows two peaks at 1250 cm-1 and 3200 cm-1, respectively. In addition to the peaks from the underlying Ni substrate, the spectra of the graphene show the characteristic D, G and 2D peak at 1350 cm-1, 1580 cm-1 and 2680 cm-1 [19-21]. The intensity ratio of the D band (1350 cm-1) to the G band (1580 cm-1) is an indication of the amount of defects in graphenes [4,5]. The ratio at the grain boundary is significantly higher (ID:IG ~1) than the value toward the center of the grain (ID:IG ~ 0.5). This is attributed to the disordered structure of the Ni grain boundaries which provides more directions for immediate sp2 bonding.

Figure A- 2. (a) An optical image of graphene on the Ni foil grain structure. (b), (c) and (d) SEM images of the vertically–oriented graphene nucleation and growth on the Ni substrate. (c) and (d) were taken on the grain boundary and in the center of the grain, respectively. (e) Raman spectra of the Ni substrate, the graphene on the grain boundary and the graphene in the center of the grain.

The optical and SEM images in Figure A-2a and A-2b show the initial growth of vertical graphenes on the Ni substrate. A patch–like pattern is observed from early nucleation and growth at the grain boundary. The Ni surface away from the grain boundary is smoother and more ordered, resulting in Volmer-Weber islands forming and growing laterally until the grains impinge. This is a much slower process than that occurring at the defects of the grain boundary. The grain size of the Ni substrate determined from the optical images has a broad distribution between 10-50 μm. SEM images in Figure A-2c and A-2d show the graphenes on the boundary and the center of the grains. The graphenes along the boundary of the grains exhibit higher, thicker and more random morphology (Figure A-2c) compared to those away from the grain boundary, which are of more uniform vertical growth and thickness (Figure A-2d). Figure A-2e shows the corresponding Raman spectra of the pure Ni surface compared to the spectra of the vertical graphene on the Ni grain boundary and towards the center of the Ni grain. The Raman spectrum of the Ni substrate shows two peaks at 1250 cm-1 and 3200 cm-1, respectively. In addition to the peaks from the underlying Ni substrate, the spectra of the graphene show the characteristic D, G and 2D peak at 1350 cm-1, 1580 cm-1 and 2680 cm-1 [4,5]. The intensity ratio of the D band (1350 cm-1) to the G band (1580 cm-1) is an indication of the amount of defects in graphenes. The ratio at the grain boundary is significantly higher (ID:IG ~1) than the value toward the center of the grain (ID:IG ~ 0.5). This is attributed to the disordered structure of the Ni grain boundaries which provides more directions for immediate sp2 attachment and growth, resulting in a random, cauliflower type of morphology (see Figure A-2c).

Figure A-3. (a) The intensity of D to G peak ratio in Raman spectra and the thickness (height) of graphene films as a function of growth time. The thickness of the films was measured from the SEM images of the VOG film on Ni/Si cross–sections.
(b) Representative SEM images of cross–sections with growth time of 10min, 25min and 40 min.

Figure A-3a shows the thickness of the sheets as a function of growth time, over the range of growth time from 10 minutes to 40 minutes. The overall height was approximately 700 nm after 10 minutes growth time and grew in a linear fashion to ~3.1 μm after 40 minutes. The growth rate is about 70-80 nm/min. The growth height was determined from SEM measurement of cleaved, vertically–oriented graphenes grown on Ni-coated Si (100) wafers (Figure A-3b). The ID/IG ratio as a function of growth time in Figure A-3a shows a significant decline from 1.5 after 10 minutes to a ratio of 0.9 after 15 minutes. The high ID/IG ratio at 10 minutes growth represents the highly disordered state of the random growth on the substrate. Then the ID/IG ratio linearly decreased to about 0.5 after 40 minutes. Calculation of the corresponding crystallite sizes ranged from 11 nm for 10 min growth to 32 nm for 40 min growth which may suggest more Stokes interaction with the upper surfaces of the taller sheets rather than the initial planar growth [6]. These results suggest the density of growing sheets had been established early on and the linear increase in height versus time was controlled by carbon ions sp2 bonding to the predominant edges. Further, the taller the sheets, the more the Raman signal comes from the more ordered graphene as compared to the contribution from

the more disordered growth near the substrate. Inspection of the regions in between these predominant sheets showed shorter, disordered embryo growth that did not survive, because of the taller sheet dominance due to the dc electric field, thus acquiring most of the ions. Previous research utilizing a single wire at 0V touching the floating substrate showed radial growth alignment emanating from the wire [7] which conclusively demonstrates growth by carbon ions in contrast to other carbon states in the plasma. In this work, the edges at 0 V in the plasma provided a similar ion focusing effect that resulted in a rate-limited, vertical sheet growth. Surface area measurements (Brunauer–Emmett–Teller (BET) method) of this growth on Si(100) wafers were conducted in previous studies and found to be ~1100 m2/g [7].

Figure A-4. Impedance phase angle versus frequency plot for an EDLC fabricated from high density vertically–oriented graphenes (20 min growth). The impedance phase angle curves from reference 2 were included for comparison.

Impedance phase angle data of a capacitor fabricated with vertically–oriented graphene (20 min growth) electrodes is shown in Figure A-4. Data of a graphene capacitor fabricated with a floating substrate and thus a lower density from reference [3] are shown for comparison. The curve is quite flat near -90° phase angle up to about 4000 Hz, indicating a nearly ideal capacitive behavior over this frequency range. At the same time, the depressed region from the previous curve at the frequency range of 1-100 Hz no longer exists. The impedance phase angle of the capacitor reaches -45° at ~30 kHz, twice as high as the value of 15 kHz reported previously and is comparable to the frequency response of the Al electrolytic capacitor [3,8]. For application in ripple filtering, the impedance phase angle of the capacitor at 120 Hz is approximately -85°, while present activated carbon EDLCs have an impedance phase angle at 120 Hz of ~ 0° [9].

Table A-1. Frequency response of the EDLCs from this work compared with previous reports.

Reference	Materials	Frequency for -45° phase angle
[4]	Activated carbon	0
[ ],[ ],[ ],[ ]	Carbon nanotube	6 Hz to 636 Hz
[ ]	Vertically-oriented graphene	100 Hz
[13]	Carbon black	1000 Hz
[12]	Electrochemically reduced graphene oxide	4200 Hz
[2],[11]	Vertically–oriented graphenes	15000 Hz
this work	Vertically–oriented graphenes	30000 Hz

Table A-1 lists the frequency at the impedance phase angle of -45° for EDLCs made from different carbon materials. To date, the devices presented here have the fastest dynamic response reported by any EDLC and is due to the very open structure of the vertically–oriented graphenes in combination with the high electronic conductivity of graphene and its low-resistance connection to the metal current collector.

Figure A-5. (a) Complex plane plot of the impedance of the graphene capacitor of 20 minute growth. (b) Capacitance versus frequency of the EDLC, assuming a series-RC circuit model.

40 minutes in 5 minute increments. A complex plane plot of the impedance data from the vertically–oriented graphene capacitor of 20 min growth is shown in Figure A-5a. The nearly vertical line of the impedance indicates that the EDLC has no porous electrode behavior. The equivalent series resistance (ESR) is 0.05 ohms. The high conductivity of the graphene sheets and the intimate ohmic contact between planar graphene and the Ni substrate both contribute to this low series resistance value. There are also absolutely no features associated with a series passive layer, which would manifest itself as a high frequency semicircle, i.e. capacitive contact to the Ni substrate. Button cell test vehicles often have this problem. Past research has shown that in a high vacuum environment, surface oxygen dissolves into the nickel bulk at elevated temperature [10], which helped to make the intimate contact between graphene and Ni substrates. Specific capacitance versus frequency is shown in Figure

A-5b. At 1 kHz, the value is 74 μF/cm2, which is 1.4 times higher than the value of 52 μF/cm2 from previous experiments [3] with the graphene grown on Ni where the substrate was electrically floating. The increase in the capacitance is from the increased density and thus increased area/edges of graphene sheets. The capacitance of the EDLC device at 120 Hz is 120 μF and the series resistance is 2.09 ohms, which yields an RC time constant of about 251 μs.

Many efforts have been made to correlate the electrochemical capacitance with the properties of carbon electrodes. The influence of properties, such as specific surface area, pore size distribution and the graphitic edge density, on the capacitors have been often discussed and are still a matter of debate [11]. To study the influence of the electrode surface area on the capacitance, vertically–oriented graphene films with increasing growth time from 10 minutes to were prepared and fabricated into symmetric capacitors.

Figure A-6. (a) Specific capacitance at 1 kHz of EDLC assembled from vertically–oriented graphenes with increasing growth time. The dotted red line is a guide to the eyes, indicating the approximately linear increase of the specific capacitance with increasing growth time. (b) Specific capacitance normalized to the sheet height decrease with the growth time.

Figure A-6a shows the specific capacitance at 1 kHz for EDLCs assembled from electrodes having vertically–oriented graphenes with increasing growth time. The capacitances were averaged from multiple devices to reduce errors from electrode wetting that is due to the highly hydrophobic nature of the graphene surface. The red line serves as the guide to the eyes, indicating the increase of the specific capacitance as a function of the growth time. As shown in Figure A-3a, the height of the graphene shows a linear increase with the growth time. As the film height increases, the area of graphene sheets increases as well. However, the height (area) increased by a factor of four, but the capacitance only doubled. Normalizing this data to the sheet height shows a decrease as a function of growth time which suggests that other effects are important, for instance, effects from graphene edges and defects. See figure A-6b.

The vertical orientation of the graphenes provides a very open structure which minimizes porosity effects and thus reduces ionic resistances within the electrode. That, in addition to the low electronic resistance of the graphene, provides a low series resistance which allows a dynamic response capable of efficient 120 Hz filtering. The irregular shaped voids formed by the vertical sheets (~200-500 nm in average dimension) are very large compared to activated carbon pores and exhibit no transmission line response behavior. The maximum specific capacitance achieved to date for a 3.1 μm tall graphene is 120 μF/cm2 at 1 kHz. Recently, Sheng et al. [12] reported that electrochemically reduced graphene oxide (ErGO) gave a specific capacitance of ~238 μF/cm2, but this was for a film thickness of 20 μm, or 6.5 times greater than the 3.1 μm tall graphenes studied here. Figure A-6a suggests that at 20 μm thick, the specific capacitance in this work would approach ~ 780 μF/cm2. Further, the frequency response in our work is significantly higher than that reported by ErGO.

The ID/IG ratio decreased with growth to a value of ~0.5 at a height of 3.1 μm indicates a significant improvement of the crystalline order because of the ionic focusing to the dominant, vertical graphene edges. Shielding of the shorter sheets eventually results in only the taller sheets preferentially intercepting the carbon ions of the plasma.

Although the capacitances of EDLCs increase with electrode surface area, the capacitance of our devices did not increase in direct proportion to the surface area. This suggests that mechanisms other than surface area were operative in the double layer charge storage. The specific capacitance normalized by the height (Figure A-6b) shows a slight but significant decrease with growth time, believed due to the edges and defect structure of the graphene sheets. A decreasing ID/IG ratio (Figure A-3a) suggests less edges and defects on samples of longer growth time, consistent with the decreasing specific capacitance per unit thickness. This implies that the edges and defects of graphene also contribute to the capacitance. In 1972, Randin et.al. reported that graphite edge planes provide capacitance of 50-70 μF/cm2 in comparison with basal planes that provide capacitance of only ~3 μF/cm2 [13,14]. These results are not universally accepted today due to possible measurement errors arising from mechanical polishing of surfaces, but this anomaly has been observed more recently by Kim et al. [15] for carbon nanofibers where they found that edge surface capacitance was more effective than basal plane surface capacitance by a factor of 3 to 5. Preliminary experiments conducted with vertically–oriented graphenes that were exposed to low energy Ar ion bombardment, following the growth of the film, showed an increase in the specific capacitance [16]. The lightly sputtered surface generates defects, like surface vacancies and dangling bonds. The defects alter the surface energy of graphenes and induce a stronger polar character of the surface sites. This could increase the ion accumulation and bond strength in the inner Helmholtz layer and thus increase the capacitance. This research area is well underway and a manuscript is in preparation.

Task 2. Increase specific capacitance by development of asymmetric electrodes.

In addition to the capacitance gain by increasing the edge density/surface area discussed in the previous task, we will continue to pursue increased capacitance with MnO2 coatings (with the mutual consent of DARPA). The coatings enhance the capacitance by adding a Faradaic component providing reversible redox reactions between the electrolyte and the electroactive

species of the coated electrode. We plan to coat CNS electrodes with Mn by RF PECVD in a partial pressure of oxygen and combine this electrode with a NiO-OH counter electrode (proprietary technology acquired from Nanotecture in England) and test the performance of the combination as an asymmetric cell. It is anticipated that the NiO-OH will provide an even greater Faradaic component and yield a substantially increased capacitance without reduction of the dynamic response.

Our results MnOx are in progress. Those with NiO-OH coatings as an asymmetric electrode showed no significant improvement in the capacitance. This work was therefore terminated.

Task C. Fabricate and characterize EDLC with a planar form factor.

A new single sheet design of a planar interdigitated EDL capacitor is described below. The figures are from a patent disclosure submitted by the College of William and Mary and JME, Incorporated. In general, the planar EDLC is comprised of interdigitated fingers of the vertically aligned graphene electrodes and an electrolyte that covers the fingers such that the final design has a planar geometry. Electrolyte covers the graphene electrode material and spans the gap between the electrode fingers. In a typical geometry, fingers would have widths in the 0.1 – 0.5 mm range and the gaps between the fingers in the 1 to 20 micrometers range. The length of the fingers can typically be 0.5 mm to 2 cm long. The height of the vertically aligned graphene sheet material can be from a fraction of micrometer to several micrometers.
Any one of a number of different electrolytes can be used. Electrolyte can be aqueous or non-aqueous. Aqueous electrolytes include KOH, H2SO4, and phosphoric acid. Gelled electrolytes can be used, for instance KOH in poly(vinyl alcohol) (PVA) or phosphoric acid in PVA.   Neat or gelled ionic liquids can be used. Electrolytes can be a solvent like propylene carbonate or acetonitrile that contains a solute (dissolved salt) like TEATFB or TEMABF4 at concentrations in the range of 0.1 M up to its solubility limit. The gelling agent can be colloidal material, for example silica, instead of a polymer like PVA. Gaps between the fingers must be spanned by the electrolyte and electrolyte must cover and wet the electrode fingers so the electrode becomes active. The advantage of using vertically aligned graphene sheets for the electrode (as opposed to activated carbon or other types of carbon for the electrode material) is that extremely high power performance EDLCs can be created. The response time of this type of EDLC, that is the characteristic charge and discharge time, can be much less than 1 ms. This type of cell is capacitive even at frequencies above 1 kHz, which would allow this to be used for filtering applications. An example is 120 Hz filtering, where the capacitor must be charged and discharged every 8.3 ms. Conventional electrolytic capacitors, such as those with a dielectric of metal oxide on a metal (aluminum for instance), are the most popular filtering capacitor today. They are known to be large and generally unreliable.   EDLCs can have higher capacitance per unit area compared with those electrolytic capacitors. EDLCs also circumvent the reliability problem common to electrolytic capacitors. The electric double layer is formed naturally at an interface when voltage is applied, and this dielectric is totally self-healing. Its breakdown then does not mean the device is destroyed, which occurs with electrolytic capacitors. There are several advantages for the planar design of an EDLC as opposed to the conventional sandwiched-structure design of current collector/electrode/separator/electrode/current collector. The planar design does not require a separator. The separator has two liabilities for an EDLC – it adds significant volume to the capacitor and also ionic resistance, which contributes to the total equivalent series resistance (ESR) of the cell. The planar structure can be much thinner than a stacked design and thus volumetrically more efficient. The planar geometry lends itself to a form factor that is better suited to many applications than the right cylinder form of a conventional capacitor. Consider, for example, placing a right-cylinder capacitor in a small cell phone package. This is much more difficult than placing a postage stamp size capacitor in the same package. One can envision major advances in performance of the described planar capacitors with further development of fabrication techniques and growth of the vertically aligned graphene sheet materials used to create the electrodes. For instance, if graphene growth temperatures can be reduced sufficiently, then planar capacitors of this type can be fabricated directly on polymer films, which are consistent with the most advanced trends--flexible electronics. See below.

Fig. C-1. Fabrication traveler

20

12

23

11   22   21

13

11

24

12

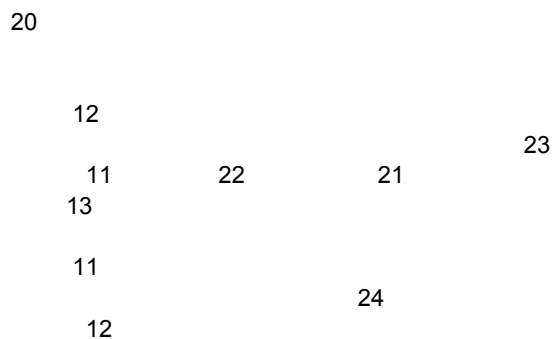Fig. C-2A.   Prior art   Fig. C-2B. Cross section of planar EDLC

20

Fig. C-3. Interdigitated square wave gap pattern created by laser ablation

+   -

Fig. C-4. Rows of interdigitated square wave gap connected in series (present invention)

Fig. C-5. Cross section of vertically oriented graphene grown on Ni/Cr/Si film with increasing growth time. Red line is the interface.

Figures C-1 through C-4 show the traveler and schematics of the square wave gap created by laser ablation. A diode-pumped 355nm laser (Tripled YAG) in a direct-write process, using a 10x microspot UV objective was used. Energy out of the laser was ~80¿J at a pulse repetition rate of 60kHz. That beam then was passed through a 770¿m aperture to achieve the desired initial spot size (~20¿m). The VOG coating was for only 20 minute growth which is a little over 1 ¿m in thickness (growth rate shown in figure C-5. The capacitive data shown below was based on this coating thickness and a 20 ¿m gap using PVA/KOH gel electrolyte and a 0.5 volt bias. Gaps approaching 1 ¿m are possible which substantially increases the capacitance.

Fig. C-6. Complex plane plot from electrochemical impedance spectroscopy (EIS) results

Fig. C-7. Bode representation from EIS. Phase angle in degrees vs frequency

In this initial effort, the results are far from optimal, but show great promise. Figure C-6 is a complex plot obtained from electrochemical impedance spectroscopy (EIS) and shows an equivalent series resistance (ESR) of 3 ohms. For proof of

concept, the laser ablation of the gap was run only long enough to achieve a modest resistance of 25 M¿¿so this can be significantly improved. In the Bode plot, a phase angle of -75 degrees was achieved at 120 Hz which indicates the use of this design to be quite promising and functional for filtering purposes. Figure C-7 shows useful capacitance even to 10 kHz and a specific capacitance of ~150 ¿F cm-2 .

Fig. C-8. EIS results. Capacitance and resistance vs frequency

Task D. Parametric study to grow CNS on aluminum substrates.

Although great progress was made on this task, it was not completed because the request for a no cost extension was denied. In order to focus and advance this new EDLC capability to a useful economic end, it is necessary to grow these capacitors on conventional substrates (e.g., Al is frequently used for electrolytic capacitors) such that they can be fabricated into capacitance levels required for military and civilian applications. This requires the utilization of aluminum substrates that can be rolled into useful capacitance levels. The major effort of the growth of CNS to date has been on Ni, Ta and other substrates at temperatures greater than 700°C. The low melting point for Al (660°C) and the low initial emissivity of Al are limitations with CH_4 as feedstock. If, however, a thin, anodized Al surface is the starting substrate (initial high emissivity changes the temperature minimally during growth) and C_2H_2 is used as the feedstock, the set of RF PECVD parameters which will allow formation of the CNS can be established. The resistance of the intermediate anodized layer can then be removed by heat treating such that some oxygen will initially evaporate as CO or CO_2 and the balance dissolve into solid solution within the Al bulk. Using acetylene, we have recently grown CNS at temperatures less than 660°C onto Si wafers[17].

The first challenge was to determine a parametric window for the growth of VOG on Al which is quite narrow due to the low melting point (660°C) and the previous parametric set using CH_4 as carbon feedstock and Ni as the substrate. The best growth results obtained to date on Ni require a heater temperature >700ºC. The approach to solve this issue was to change the feedstock from CH_4 to C_2H_2 which allows twice the carbon atoms and ions in the plasma and results in twice the growth rate. Further, a parametric study to adjust all the controlling parameters to lower the growth temperature to below 660ºC was required. In order to achieve the precision necessary to accomplish this task, a number of improvements to the present growth facility were implemented. Replacement of dial type current and voltage indicators with more accurate digital meters was completed. The existing flow controllers, which are a mix of old, un-calibrated instruments from instrument storage that had higher full scale flow ranges (notoriously inaccurate at low flow rates), to new calibrated MKS versions for CH_4, C_2H_2, Ar and H_2 was completed. Also, a system for gas analysis using an SRS 100 mass spectrometer (with separate differential pumping) was added. This will allow direct line of sight assessment of plasma species.

A Langmuir probe for RF plasma was also designed (not yet fabricated). With the mass spectrometer facility, we can determine the density of each ion specie in the plasma so that, along with the Langmuir probe, we have good plasma characterization. A new Alcatel vacuum pump with lower ultimate pressure was also installed to replace the old rotary vane pump. Mechanically polished flat Ta masks were employed in combination with optically flat Al_2O_3 platens to improve the heat transfer over the substrate surface of existing substrate heater. This insured uniform temperature over the metal foil substrate during growth. Although the melting point of Ni is not a concern, a hot spot on an Al substrate is a concern because if any part of the Al melted it would spread over the entire foil immediately, which destroys the film and substrate.
Figure D-1a shows the morphology achieved with the heretofore utilized procedure of allowing the substrate to float with the plasma. Although we have taken most of the previous data with this condition, a simple experiment with grounding the substrate with a single wire resulted in a radial growth around the wire with excellent verticality. This clearly showed that the growth was from ions in the plasma. The transfer of that behavior to uniformly cover a substrate surface was not immediately obvious. Our first attempt in doing this was with a grounded high transmission Ni electroformed grid lying flush against the Ni substrate. One difficulty was insuring that the grid was planar and touched the substrate at every surface point. A second difficulty was having the Ni grid diffusion bond with the substrate. We then went to a stiffer W grid under the mask shown in figure A-1. Figure D-1b shows the substantial improvement in verticality and the substantial increase in density. This became the procedure for all the work presented in this report. At present, we are testing this mode of growth for capacitance properties using a more negative bias to see if further improvement can be obtained. Experiments with negatively biased high transmission W grid mesh sizes of (4 lines per mm and 2 lines per mm) placed on the substrate surface are presently being studied and show a further increase in the sheet density, but electronic problems with the RF, overwhelming the dc power supply, require further electronic refinement (Faraday cage). The plasma in the center of the mesh elements to the substrate surface or to the mesh edge is ¿ ~ 125 micrometers and the mean free path at 100 mTorr (133 mbar) of the CH_4/H_2 plasma is ¿ ~ 500 micrometers. This results in an unimpeded ion trajectory to the substrate and is why the growth predominantly occurs as a result of ion transport (C^+, CH^+, CH_2^+, CH_3^+ and CH_4^+) as opposed to neutrals.
Following temperature calibration with heater current, the first result of growth using this improved system was recently done

with C2H2 on a Ni substrate (0V potential and no grid) at low temperature (600ºC). See figure D-2. Although the sheet thicknesses are slightly larger than achieved with CH4, the films appear to be of excellent morphology with good verticality. This initial work is quite promising and suggests a high probability of success with Al substrates. The high purity (99.999%) polycrystalline Al substrates are in hand and experiments with these foils are imminent, but parametric studies with Ni must first be done to optimize the growth morphology at the lowest temperature possible. This is necessary to reduce the possibility of a catastrophic failure with the Al (melting would destroy the substrate heater).

The Ni work is also highly promising and should provide an excellent publishable result.

Relevance to the Army

The projected reduction in weight and volume over SOA capacitor elements used in power electronics equipment is greater than a factor of 10. Presently, we have achieved a factor of 6. These savings are applicable to all branches of the military as well as the civilian sector. This translates into substantial reduction in voltage sources for equipment required for each marine and soldier. Furthermore, this advance alters weight and volume constraints for all new military system designs, especially orbital requirements for satellites and payloads. It should also impact the weight and volume of aircraft electronics.

Collaborations and technology transfer

We worked with Professor Steve George in the Chemistry Department at the University of Colorado to use Atomic Layer Deposition to determine the contribution of edge density as compared to the surface area. Professor George was sent 10 pairs of VOG/Ni with plans to coat them with MnOx. He did preliminary work with ALD on Al2O3/SiO2 (glassy) substrates. Growth on VOG is underway.

We have received all Ni foils from Nanotecture in Southampton, England for NiO(OH) coatings on edges of carbon nanosheets to test for improved capacitance, but observed no significant improvement.

Journal publications from this research

M. Cai, R.A. Outlaw, S.M. Butler and J.M Miller, "A high density of vertically oriented graphenes for EDL supercapacitors", Carbon, 50 (2012) 5481

References

1.   Zhao, X., Outlaw, R.A., Wang, J.J., Zhu, M., Smith, G.A. and Holloway, B.C., "Thermal Desorption of Hydrogen from Carbon Nanosheets", J. Chem. Phys. 124 (2006) 194704 .
2.   Wang, J et.al.., "Synthesis of carbon nanosheets by inductively coupled radio frequency plasma enhanced chemical vapor deposition", Carbon 42 (2004) 2867-2872.
3.   Miller, J.M., Outlaw, R.A. and Holloway, B.C., "Graphene Double Layer Capacitor Capable of Efficient AC Filtering", Science, 329 (2010) 1637.
4.   Ferrari, A.C., Robertson, J., "Interpretation of Raman spectra of disordered and amorphous carbon", Phys. Rev. B, 61 2000) 14095.
5.   Pimenta, M.A., Dresselhaus, G, Dresselhaus, M.S., Cancado, L.G., Jorio, A., Saito, R., "Studying disorder in graphite based systems by Raman spectroscopy", Phys. Chem. Chem. Phys. 9(2007)1276.
6.   Cancado, L.G., Takai, K., Enoki, T., Endo, M., Mizusaki, H., "General equation for the determination of the crystallite size of nanographite by Raman spectroscopy", Appl. Phys. Lett. 88(2006)163106.
7.   Zhu, M., Wang, J., Holloway, B.C., Outlaw, R.A., Zhao, X., Hou, K., Shutthanandan, V. and Manos, D.M., "A Mechanism for Carbon Nanosheet Formation", Carbon, 45 (2007) 2229
8.   Miller, J.M. , Outlaw, R.A. and Holloway, B.C., "Graphene Double Layer Capacitor with ac Filtering Performance",

Electrochimica Acta, 56 (1011)10443

9. Pandolfo, G., Hollenkamp, A.F., "Carbon properties and their role in supercapacitors", J Power Sources;157(2006)11–27.

10. Holloway, P. H.; and Outlaw, R. A.: "The Effect of Temperature Upon NiO Formation and Oxygen Removal on Ni (110)". Surface Science, 12A(1981)1809

11. Frackowiak, E., Béguin, F., "Carbon materials for the electrochemical storage of energy in capacitors". Carbon 39(2001) 937

12. Sheng K, Sun Y, Li C, Yuan W, Shi G. Ultrahigh-rate supercapacitors based on eletrochemically reduced graphene oxide for ac line-filtering. Sci Rep 2012;2:247.

13. Randin, J.P., Yeager, E. "Differential capacitance study of stress annealed pyrolytic graphite electrodes", J Electrochem Soc.;118(1971)711.

14. Randin, J.P, Yeager, E. "Differential capacitance study on the basal plane of stress-annealed pyrolytic graphite". J Electroanal Chem Interfacial Electrochem; 36(1972)257.

15. Kim, T., Lim, S., Kwon, K., Hong, S.H., Qiao, W, Rhee, C.K., et al., "Electrochemical capacitances of well-defined carbon surfaces". Langmuir 22(2006)9086.

16. Cai, M., Outlaw, R.A., Butler, S.M., and Miller, J.M., Carbon (in preparation).

17. Zhu, M., Outlaw, R.A., Bagge-Hansen, M., Chen, H.J. and Manos, D.M., "Field Emission of CNS from C2H2 feedstock", Carbon, 49 (2011) 2526

Technology Transfer

Final Report

Vertically Oriented Graphene Electrochemical Double Layer Capacitor with Very Fast Dynamic Response

PI – Professor Ronald A. Outlaw
Department of Applied Science
College of William and Mary
Williamsburg, Virginia 23187-8795

Introduction:

Activated carbon materials are expected to play a crucial role in supercapacitor technology. To date, they are the most preferred choice because they can be processed to have exceptionally high surface area, relatively high electric conductivity and are reasonably priced. This work was to improve the morphological structure of vertically oriented graphene (VOG), also called carbon nanosheets (CNS), to a higher density of taller sheets so that the total surface area is substantially increased, which increases capacitance, and more verticality to improve response time. An increase in the surface area of a factor of four resulted in only a factor of two increase in capacitance. Parametric studies in radio frequency plasma enhanced chemical vapor deposition (RF PECVD) growth and the use of gridded mesh on the substrate with a bias voltage provided higher density growth of the vertically oriented graphitic sheets. It was anticipated that, eventually, there would be a sheet density and sheet height that substantially impacts the dynamic response because of decreasing electrolyte conductance, but that was not yet observed. This optimal point that maximizes capacitance without significant loss of dynamic response is a primary growth objective. Studies to further increase the capacitance with the use of coatings, such as oxidized Mn and Ru, or the NiO-OH coated asymmetric electrode were conducted for an anticipated synergistic impact on electrical double layer capacitance (EDLC) properties, but only marginal impact was observed. Finally, edge and defects in the sheets also have been found to increase capacitance in similar structures. This suggests that (by growth, chemical alteration or by ion bombardment) an increased edge/defect density that does not significantly inhibit electron transport is an important objective. This was studied using Ar ion bombardment to increase defects.

Approach:

The following is the proposal statement of work tasks with the achievements accomplished toward completing these tasks.

**Task A. Optimize capacitance of vertically oriented carbon nanosheets electrodes
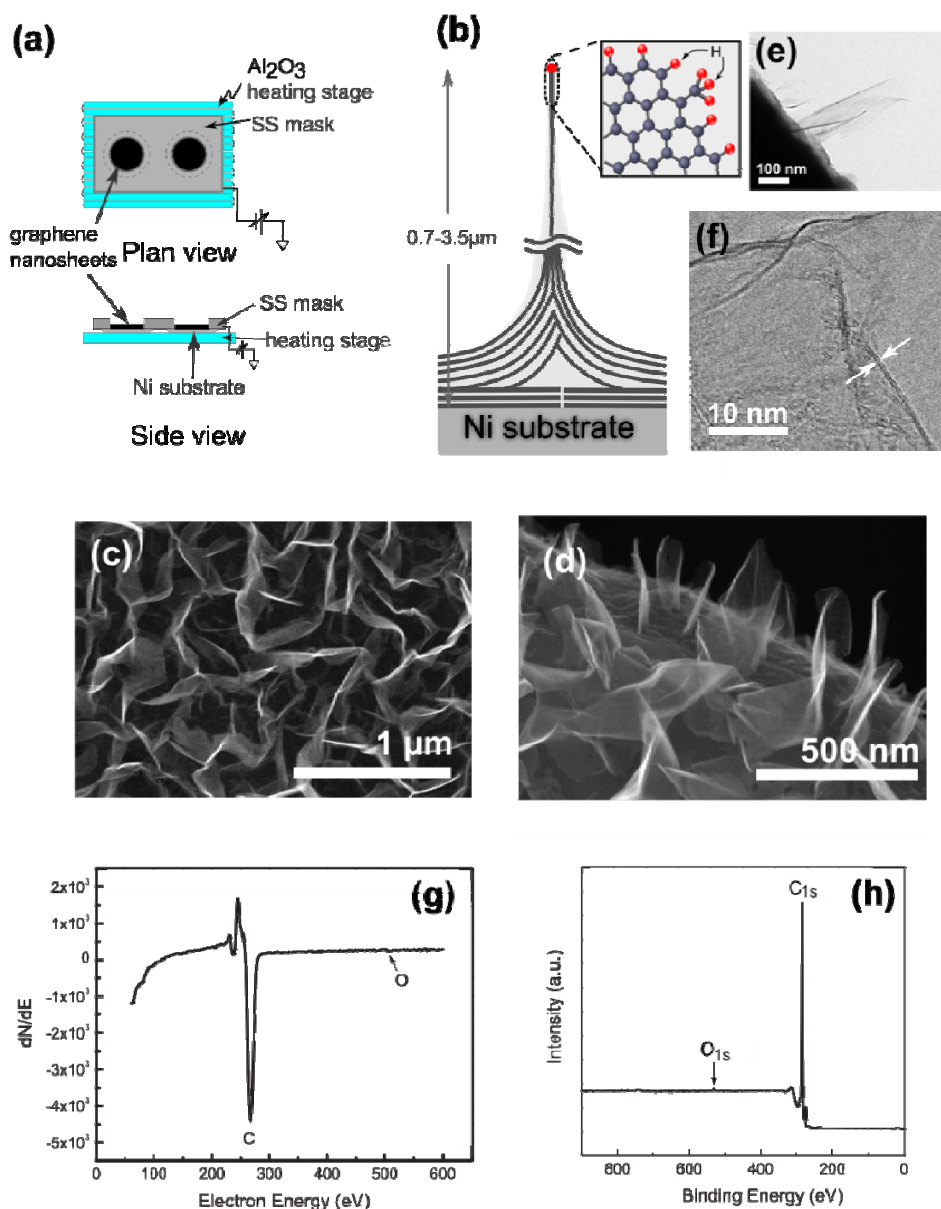Increase capacitance by maximizing the charge carrier density of the graphene.**

Figure A-1. (a) Schematics of the plan and side view of the experimental setup. The Ni substrate and the stainless steel (SS) mask were grounded. (b) A schematic of the structure of vertically–oriented graphenes on Ni substrate near the base [11]. Edges are terminated with 1-3 hydrogen atoms. (c) SEM image of vertically–oriented graphenes, plan view. (d) SEM glancing incidence image showing the thickness of the vertically–oriented graphenes (e) TEM image showing a single sheet of the vertically-oriented graphenes (f) HRTEM of graphenes showing double parallel fringes (indicating by arrows) with a distance of 0.37nm at the edge. (g) AES and (h) XPS spectra of vertically-oriented graphenes showing the very high purity of the sheets.

2

The morphology and structure of vertically–oriented graphenes on the Ni substrate are shown in Figure A-1c and A-1d. The initial Volmer-Weber planar growth of two-dimensional graphitic islands on the Ni substrate ultimately impinge on each other, and then push the sp^2 bonds upward. The dissociated carbon in the plasma then continuously provides ions and atoms to the vertically growing hexagonal lattice. The basal layer is approximately 10 nm thick. After 20-min growth, the resulting coating was comprised of vertically–oriented graphenes, ~1.5 μm high with a cross-section <1 nm thick (see Figure A-1b), having an average thickness of about one to three layers. Figure A-1e is a low magnification image showing a sheet grown vertically on the substrate. Two parallel fringes were observed from the HRTEM (Figure A-1f) at the edge of graphenes where it is bent and folded back over itself. The number of the fringes indicates that this particular sheet consist of 2 atomic layers. Most vertical sheets terminate in a single graphene sheet. The AES and XPS spectra of graphenes were shown in Figure 1g and Figure A-1f. It can be seen that, besides the C feature, only a very small amount of oxygen was detected 9 The XPS spectrum also shows predominantly C feature with a negligible amount of O due to the ambient exposure. These results indicate that the vertically-oriented graphene sheets are virtually free of contamination (<1%). Previous temperature desorption spectroscopy does show a substantial of intercalated hydrogen [1].

When the substrate is electrically floating with the plasma, it is likely that the substrate rises to near the plasma electron/ion potential and gives a much more irregular and random morphology. However, when the substrate is grounded, an applied potential between the plasma and the films creates a local dc electric field component that more efficiently directs the movement of ions to the tallest sheets and results in a growth of graphene that is taller and has a higher sheet density compared to previous work [2, 3]. All data presented in this paper were based on the Ni substrates at 0 V.

The optical and SEM images in Figure A-2a and A-2b show the initial growth of vertical graphenes on the Ni substrate. A patch–like pattern is observed from early nucleation and growth at the grain boundary. The Ni surface away from the grain boundary is smoother and more ordered, resulting in Volmer-Weber islands forming and growing laterally until the grains impinge. This is a much slower process than that occurring at the defects of the grain boundary. The grain size of the Ni substrate determined from the optical images has a broad distribution between 10-50 μm. SEM images in Figure A-2c and A-2d show the graphenes on the boundary and the center of the grains. The graphenes along the boundary of the grains exhibit higher, thicker and more random morphology (Figure A-2c) compared to those away from the grain boundary, which are of more uniform vertical growth and thickness (Figure A-2d). Figure A-2e shows the corresponding Raman spectra of the pure Ni surface compared to the spectra of the vertical graphene on the Ni grain boundary and towards the center of the Ni grain. The Raman spectrum of the Ni substrate shows two peaks at 1250 cm-1 and 3200 cm-1, respectively. In addition to the peaks from the underlying Ni substrate, the spectra of the graphene show the characteristic D, G and 2D peak at 1350 cm-1, 1580 cm-1 and 2680 cm-1 [19-21]. The intensity ratio of the D band (1350 cm-1) to the G band (1580 cm-1) is an indication of the amount of defects in graphenes [4,5]. The ratio at the grain boundary is significantly higher ($I_D:I_G$ ~1) than the value toward the center of the grain ($I_D:I_G$ ~ 0.5). This is attributed to the disordered structure of the Ni grain boundaries which provides more directions for immediate sp^2 bonding.
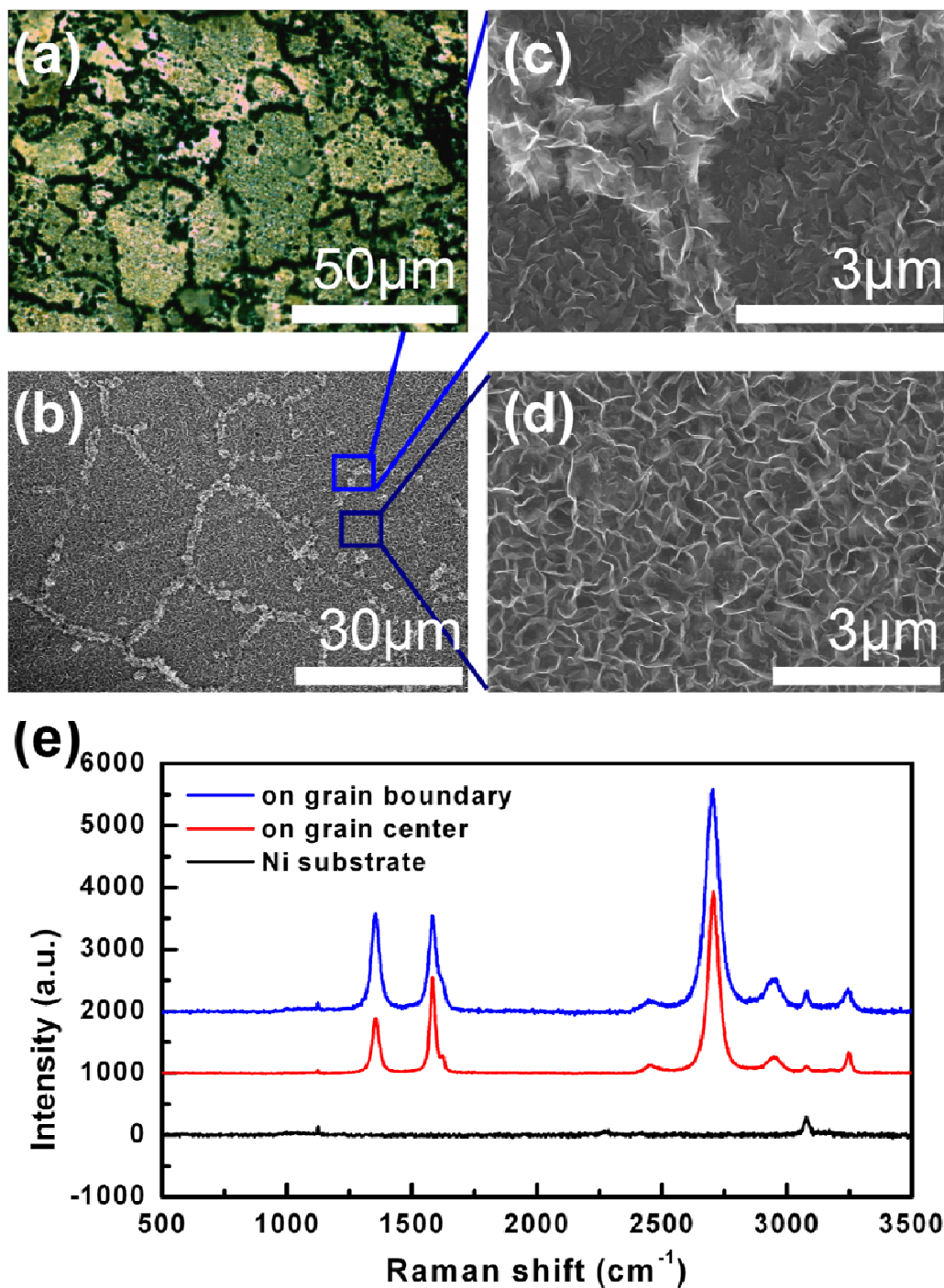
3

Figure A- 1. (a) An optical image of graphene on the Ni foil grain structure. (b), (c) and (d) SEM images of the vertically–oriented graphene nucleation and growth on the Ni substrate. (c) and (d) were taken on the grain boundary and in the center of the grain, respectively. (e) Raman spectra of the Ni substrate, the graphene on the grain boundary and the graphene in the center of the grain.

The optical and SEM images in Figure A-2a and A-2b show the initial growth of vertical graphenes on the Ni substrate. A patch–like pattern is observed from early nucleation and growth at the grain boundary. The Ni surface away from the grain boundary is smoother and more ordered, resulting in Volmer-Weber islands forming and growing laterally until the grains impinge. This is a much slower process than that occurring at the defects of the grain boundary. The grain size of the Ni substrate determined from the optical images has a broad distribution between 10-50 μm. SEM images in Figure A-2c and A-2d show the graphenes on the boundary and the center of the grains. The graphenes along the boundary of the grains exhibit higher, thicker and more random morphology (Figure A-2c) compared to those away from the grain boundary, which are of more uniform vertical growth and thickness (Figure A-2d). Figure A-2e shows the corresponding Raman spectra of the pure Ni surface compared to the spectra of the vertical graphene on the Ni grain boundary and towards the center of the Ni grain. The Raman spectrum of the Ni substrate shows two peaks at 1250 cm-1 and 3200 cm-1, respectively. In addition to the peaks from the underlying Ni substrate, the spectra of the graphene show the characteristic D, G and 2D peak at 1350 cm-1, 1580 cm-1 and 2680 cm-1 [4,5]. The intensity ratio of the D band (1350 cm-1) to the G band (1580 cm-1) is an indication of the amount of defects in graphenes. The ratio at the grain boundary is significantly higher (I_D:I_G ~1) than the value toward the center of the grain (I_D:I_G ~ 0.5). This is attributed to the disordered structure of the Ni grain boundaries which provides more directions for immediate sp^2 attachment and growth, resulting in a random, cauliflower type of morphology (see Figure A-2c).
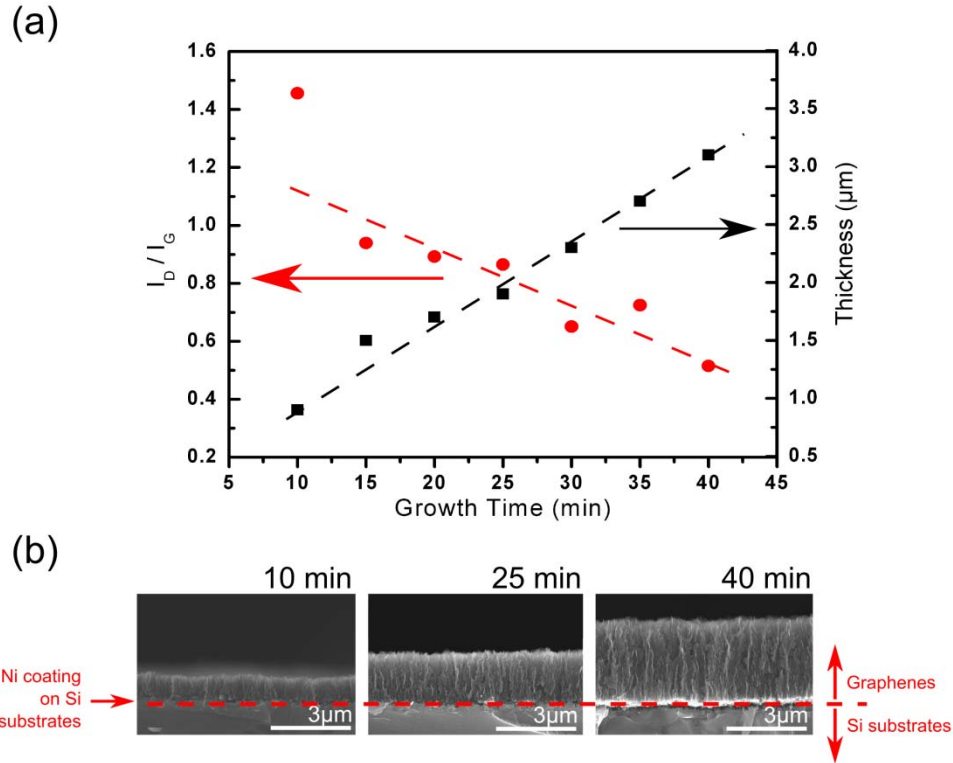
(a)

(b)

Figure A-2. (a) The intensity of D to G peak ratio in Raman spectra and the thickness (height) of graphene films as a function of growth time. The thickness of the films was measured from the SEM images of the VOG film on Ni/Si cross–sections.
(b) Representative SEM images of cross–sections with growth time of 10min, 25min and 40 min.

Figure A-3a shows the thickness of the sheets as a function of growth time, over the range of growth time from 10 minutes to 40 minutes. The overall height was approximately 700 nm after 10 minutes growth time and grew in a linear fashion to ~3.1 μm after 40 minutes. The growth rate is about 70-80 nm/min. The growth height was determined from SEM measurement of cleaved, vertically–oriented graphenes grown on Ni-coated Si (100) wafers (Figure A-3b). The I_D/I_G ratio as a function of growth time in Figure A-3a shows a significant decline from 1.5 after 10 minutes to a ratio of 0.9 after 15 minutes. The high I_D/I_G ratio at 10 minutes growth represents the highly disordered state of the random growth on the substrate. Then the I_D/I_G ratio linearly decreased to about 0.5 after 40 minutes. Calculation of the corresponding crystallite sizes ranged from 11 nm for 10 min growth to 32 nm for 40 min growth which may suggest more Stokes interaction with the upper surfaces of the taller sheets rather than the initial planar growth [6]. These results suggest the density of growing sheets had been established early on and the linear increase in height versus time was controlled by carbon ions sp^2 bonding to the predominant edges. Further, the taller the sheets, the more the Raman signal comes from the more ordered graphene as compared to the contribution from the more disordered growth near the substrate. Inspection of the regions in between these predominant sheets showed shorter, disordered embryo growth that did not survive, because of the taller sheet dominance due to the dc electric field, thus acquiring most of the ions. Previous research utilizing a single wire at 0V touching the floating substrate showed radial growth alignment emanating from the wire [7] which conclusively demonstrates growth by carbon ions in contrast to other carbon states in the plasma. In this work, the edges at 0 V in the plasma provided a similar ion focusing effect that resulted in a rate-limited, vertical sheet growth. Surface area measurements (Brunauer–Emmett–Teller (BET) method) of this growth on Si(100) wafers were conducted in previous studies and found to be ~1100 m^2/g [7].
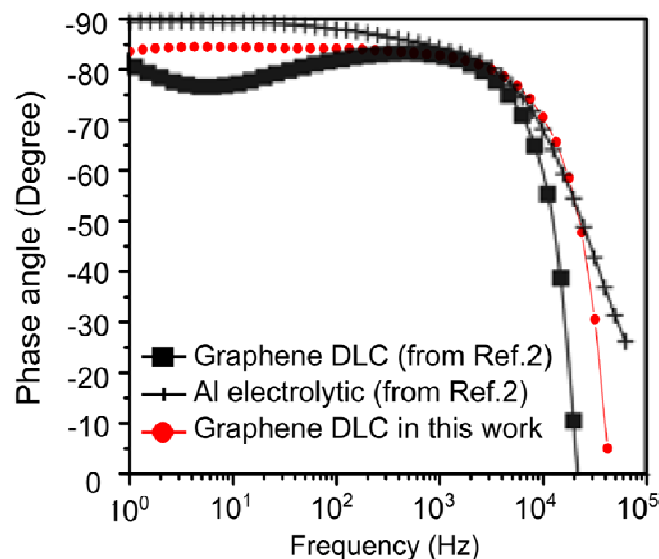

Figure A-3. Impedance phase angle versus frequency plot for an EDLC fabricated from high density vertically–oriented graphenes (20 min growth). The impedance phase angle curves from reference 2 were included for comparison.

Impedance phase angle data of a capacitor fabricated with vertically–oriented graphene (20 min growth) electrodes is shown in Figure A-4. Data of a graphene capacitor fabricated with a floating substrate and thus a lower density from reference [3] are shown for comparison. The curve is quite flat near -90° phase angle up to about 4000 Hz, indicating a nearly ideal capacitive behavior over this frequency range. At the same time, the depressed region from the previous curve at the frequency range of 1-100 Hz no longer exists. The impedance phase angle of the capacitor reaches -45° at ~30 kHz, twice as high as the value of 15 kHz reported previously and is comparable to the frequency response of the Al electrolytic capacitor [3,8]. For application in ripple filtering, the impedance phase angle of the capacitor at 120 Hz is approximately -85°, while present activated carbon EDLCs have an impedance phase angle at 120 Hz of ~ 0° [9].

Table A-1. Frequency response of the EDLCs from this work compared with previous reports.

Reference	Materials	Frequency for -45° phase angle
[Error! Bookmark not defined.]	**Activated carbon**	**0**
[i],[ii],[iii],[iv]	**Carbon nanotube**	**6 Hz to 636 Hz**
[v]	**Vertically-oriented graphene**	**100 Hz**
[Error! Bookmark not defined.]	**Carbon black**	**1000 Hz**
[Error! Bookmark not defined.]	**Electrochemically reduced graphene oxide**	**4200 Hz**
[Error! Bookmark not defined.],[Error! Bookmark not defined.]	**Vertically–oriented graphenes**	**15000 Hz**
this work	**Vertically–oriented graphenes**	**30000 Hz**

Table A-1 lists the frequency at the impedance phase angle of -45° for EDLCs made from different carbon materials. To date, the devices presented here have the fastest dynamic response reported by any EDLC and is due to the very open structure of the vertically–oriented graphenes in combination with the high electronic conductivity of graphene and its low-resistance connection to the metal current collector.
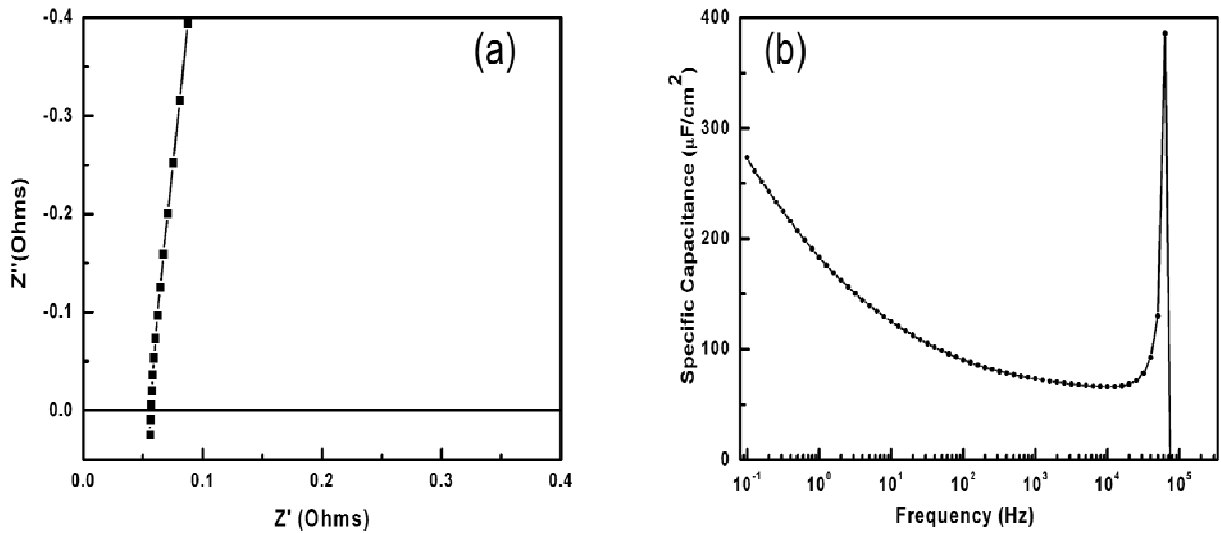
Figure A-4. (a) Complex plane plot of the impedance of the graphene capacitor of 20 minute growth. (b) Capacitance versus frequency of the EDLC, assuming a series-RC circuit model.

40 minutes in 5 minute increments. A complex plane plot of the impedance data from the vertically–oriented graphene capacitor of 20 min growth is shown in Figure A-5a. The nearly vertical line of the impedance indicates that the EDLC has no porous electrode behavior. The equivalent series resistance (ESR) is 0.05 ohms. The high conductivity of the graphene sheets and the intimate ohmic contact between planar graphene and the Ni substrate both contribute to this low series resistance value. There are also absolutely no features associated with a series passive layer, which would manifest itself as a high frequency semicircle, i.e. capacitive contact to the Ni substrate. Button cell test vehicles often have this problem. Past research has shown that in a high vacuum environment, surface oxygen dissolves into the nickel bulk at elevated temperature [10], which helped to make the intimate contact between graphene and Ni substrates. Specific capacitance versus frequency is shown in Figure A-5b. At 1 kHz, the value is 74 $\mu F/cm^2$, which is 1.4 times higher than the value of 52 $\mu F/cm^2$ from previous experiments [3] with the graphene grown on Ni where the substrate was electrically floating. The increase in the capacitance is from the increased density and thus increased area/edges of graphene sheets. The capacitance of the EDLC device at 120 Hz is 120 μF and the series resistance is 2.09 ohms, which yields an RC time constant of about 251 μs.

8

Many efforts have been made to correlate the electrochemical capacitance with the properties of carbon electrodes. The influence of properties, such as specific surface area, pore size distribution and the graphitic edge density, on the capacitors have been often discussed and are still a matter of debate [11]. To study the influence of the electrode surface area on the capacitance, vertically–oriented graphene films with increasing growth time from 10 minutes to were prepared and fabricated into symmetric capacitors.

Figure A-5. (a) Specific capacitance at 1 kHz of EDLC assembled from vertically–oriented graphenes with increasing growth time. The dotted red line is a guide to the eyes, indicating the approximately linear increase of the specific capacitance with increasing growth time. (b) Specific capacitance normalized to the sheet height decrease with the growth time.

Figure A-6a shows the specific capacitance at 1 kHz for EDLCs assembled from electrodes having vertically–oriented graphenes with increasing growth time. The capacitances were averaged from multiple devices to reduce errors from electrode wetting that is due to the highly hydrophobic nature of the graphene surface. The red line serves as the guide to the eyes, indicating the increase of the specific capacitance as a function of the growth time. As shown in Figure A-3a, the height of the graphene shows a linear increase with the growth time. As the film height increases, the area of graphene sheets increases as well. However, the height (area) increased by a factor of four, but the capacitance only doubled. Normalizing this data to the sheet height shows a decrease as a function of growth time which suggests that other effects are important, for instance, effects from graphene edges and defects. See figure A-6b.

9

The vertical orientation of the graphenes provides a very open structure which minimizes porosity effects and thus reduces ionic resistances within the electrode. That, in addition to the low electronic resistance of the graphene, provides a low series resistance which allows a dynamic response capable of efficient 120 Hz filtering. The irregular shaped voids formed by the vertical sheets (~200-500 nm in average dimension) are very large compared to activated carbon pores and exhibit no transmission line response behavior. The maximum specific capacitance achieved to date for a 3.1 μm tall graphene is 120 $\mu F/cm^2$ at 1 kHz. Recently, Sheng et al. [12] reported that electrochemically reduced graphene oxide (ErGO) gave a specific capacitance of ~238 $\mu F/cm^2$, but this was for a film thickness of 20 μm, or 6.5 times greater than the 3.1 μm tall graphenes studied here. Figure A-6a suggests that at 20 μm thick, the specific capacitance in this work would approach ~ 780 $\mu F/cm^2$. Further, the frequency response in our work is significantly higher than that reported by ErGO.

The I_D/I_G ratio decreased with growth to a value of ~0.5 at a height of 3.1 μm indicates a significant improvement of the crystalline order because of the ionic focusing to the dominant, vertical graphene edges. Shielding of the shorter sheets eventually results in only the taller sheets preferentially intercepting the carbon ions of the plasma.

Although the capacitances of EDLCs increase with electrode surface area, the capacitance of our devices did not increase in direct proportion to the surface area. This suggests that mechanisms other than surface area were operative in the double layer charge storage. The specific capacitance normalized by the height (Figure A-6b) shows a slight but significant decrease with growth time, believed due to the edges and defect structure of the graphene sheets. A decreasing I_D/I_G ratio (Figure A-3a) suggests less edges and defects on samples of longer growth time, consistent with the decreasing specific capacitance per unit thickness. This implies that the edges and defects of graphene also contribute to the capacitance. In 1972, Randin et.al. reported that graphite edge planes provide capacitance of 50-70 $\mu F/cm^2$ in comparison with basal planes that provide capacitance of only ~3 $\mu F/cm^2$ [13,14]. These results are not universally accepted today due to possible measurement errors arising from mechanical polishing of surfaces, but this anomaly has been observed more recently by Kim et al. [**Error! Bookmark not defined.**] for carbon nanofibers where they found that edge surface capacitance was more effective than basal plane surface capacitance by a factor of 3 to 5. Preliminary experiments conducted with vertically–oriented graphenes that were exposed to low energy Ar ion bombardment, following the growth of the film, showed an increase in the specific capacitance [16]. The lightly sputtered surface generates defects, like surface vacancies and dangling bonds. The defects alter the surface energy of graphenes and induce a stronger polar character of the surface sites. This could increase the ion accumulation and bond strength in the inner Helmholtz layer and thus increase the capacitance. This research area is well underway and a manuscript is in preparation.

Task 2. Increase specific capacitance by development of asymmetric electrodes.

In addition to the capacitance gain by increasing the edge density/surface area discussed in the previous task, we will continue to pursue increased capacitance with MnO_2 coatings (with the mutual consent of DARPA). The coatings enhance the capacitance by adding a Faradaic component providing reversible redox reactions between the electrolyte and the electroactive species of the coated electrode. We plan to coat CNS electrodes with Mn by RF PECVD in a partial pressure of oxygen and combine this electrode with a NiO-OH counter electrode (proprietary technology

10

acquired from Nanotecture in England) and test the performance of the combination as an asymmetric cell. It is anticipated that the NiO-OH will provide an even greater Faradaic component and yield a substantially increased capacitance without reduction of the dynamic response.
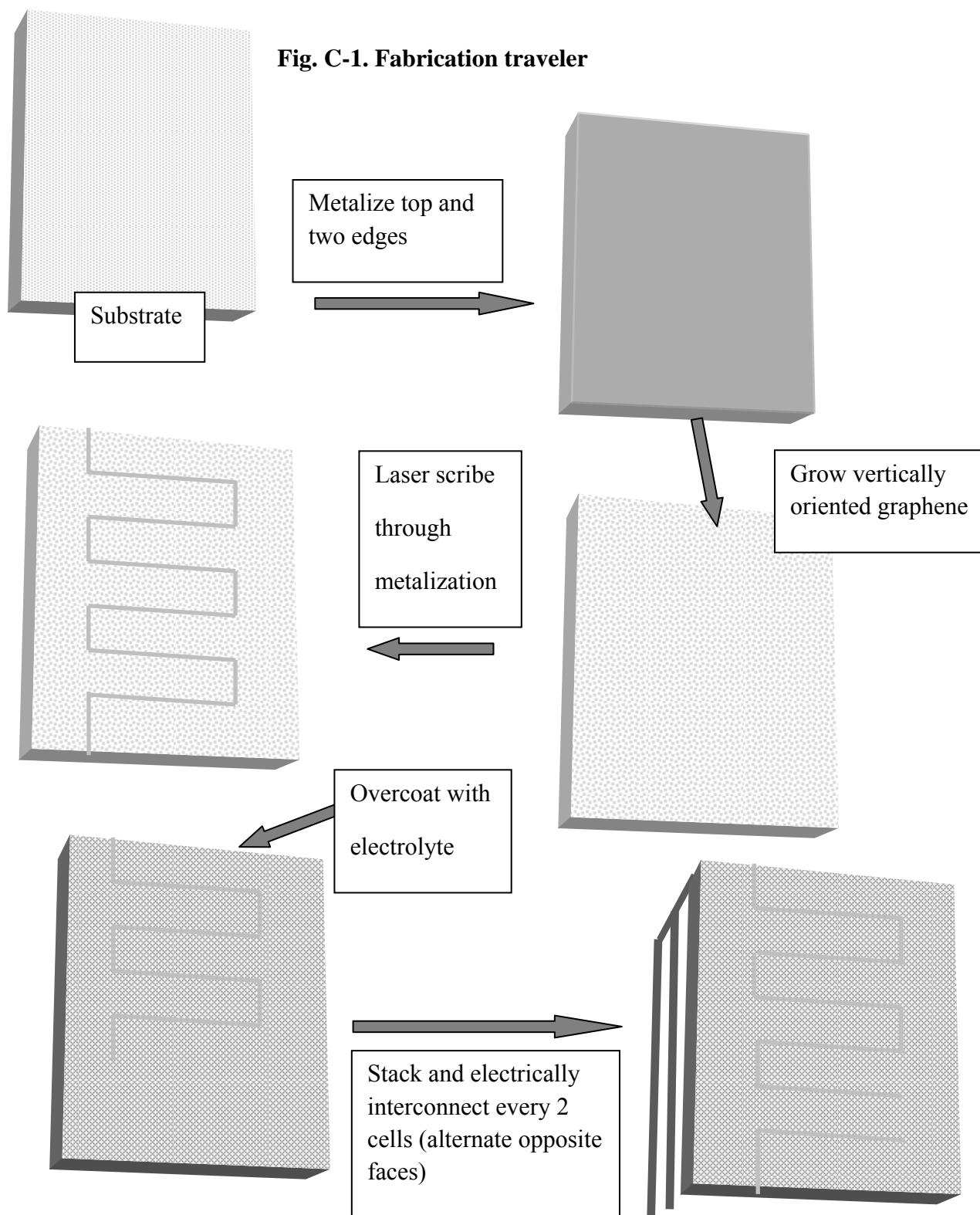
Our results MnOx are in progress. Those with NiO-OH coatings as an asymmetric electrode showed no significant improvement in the capacitance. This work was therefore terminated.

Task C. Fabricate and characterize EDLC with a planar form factor.

A new single sheet design of a planar interdigitated EDL capacitor is described below. The figures are from a patent disclosure submitted by the College of William and Mary and JME, Incorporated. In general, the planar EDLC is comprised of interdigitated fingers of the vertically aligned graphene electrodes and an electrolyte that covers the fingers such that the final design has a planar geometry. Electrolyte covers the graphene electrode material and spans the gap between the electrode fingers. In a typical geometry, fingers would have widths in the 0.1 – 0.5 mm range and the gaps between the fingers in the 1 to 20 micrometers range. The length of the fingers can typically be 0.5 mm to 2 cm long. The height of the vertically aligned graphene sheet material can be from a fraction of micrometer to several micrometers.

Any one of a number of different electrolytes can be used. Electrolyte can be aqueous or non-aqueous. Aqueous electrolytes include KOH, H_2SO_4, and phosphoric acid. Gelled electrolytes can be used, for instance KOH in poly(vinyl alcohol) (PVA) or phosphoric acid in PVA.   Neat or gelled ionic liquids can be used. Electrolytes can be a solvent like propylene carbonate or acetonitrile that contains a solute (dissolved salt) like TEATFB or $TEMABF_4$ at concentrations in the range of 0.1 M up to its solubility limit. The gelling agent can be colloidal material, for example silica, instead of a polymer like PVA. Gaps between the fingers must be spanned by the electrolyte and electrolyte must cover and wet the electrode fingers so the electrode becomes active. The advantage of using vertically aligned graphene sheets for the electrode (as opposed to activated carbon or other types of carbon for the electrode material) is that extremely high power performance EDLCs can be created. The response time of this type of EDLC, that is the characteristic charge and discharge time, can be much less than 1 ms. This type of cell is capacitive even at frequencies above 1 kHz, which would allow this to be used for filtering applications. An example is 120 Hz filtering, where the capacitor must be charged and discharged every 8.3 ms. Conventional electrolytic capacitors, such as those with a dielectric of metal oxide on a metal (aluminum for instance), are the most popular filtering capacitor today. They are known to be large and generally unreliable.   EDLCs can have higher capacitance per unit area compared with those electrolytic capacitors. EDLCs also circumvent the reliability problem common to electrolytic capacitors. The electric double layer is formed naturally at an interface when voltage is applied, and this dielectric is totally self-healing. Its breakdown then does not mean the device is destroyed, which occurs with electrolytic capacitors. There are several advantages for the planar design of an EDLC as opposed to the conventional sandwiched-structure design of current collector/electrode/separator/ electrode/current collector. The planar design does not require a separator. The separator has two liabilities for an EDLC – it adds significant volume to the capacitor and also ionic resistance, which contributes to the total equivalent series resistance (ESR) of the cell. The planar structure can be much thinner than a stacked design and thus volumetrically more efficient. The planar geometry lends itself to a form

11

factor that is better suited to many applications than the right cylinder form of a conventional capacitor. Consider, for example, placing a right-cylinder capacitor in a small cell phone package. This is much more difficult than placing a postage stamp size capacitor in the same package. One can envision major advances in performance of the described planar capacitors with further development of fabrication techniques and growth of the vertically aligned graphene sheet materials used to create the electrodes. For instance, if graphene growth temperatures can be reduced sufficiently, then planar capacitors of this type can be fabricated directly on polymer films, which are consistent with the most advanced trends--flexible electronics. See below.
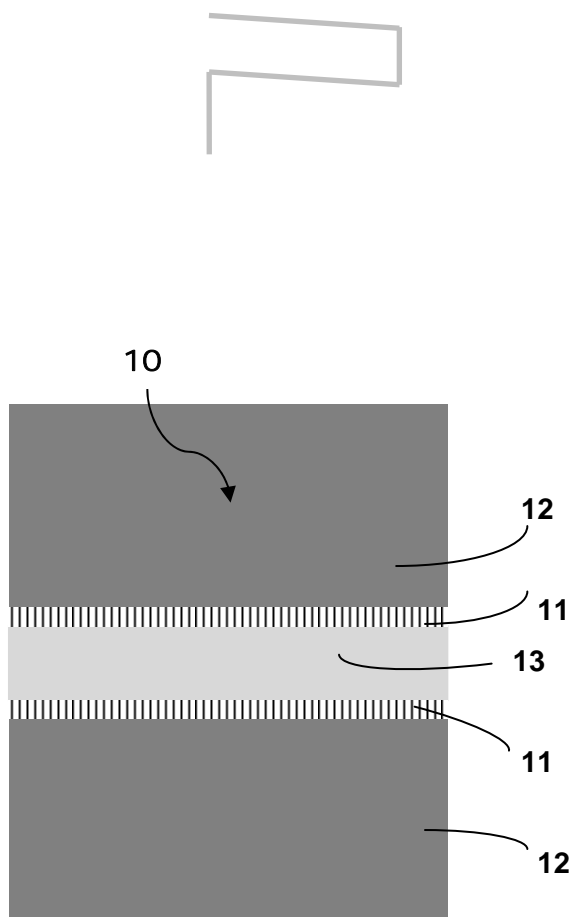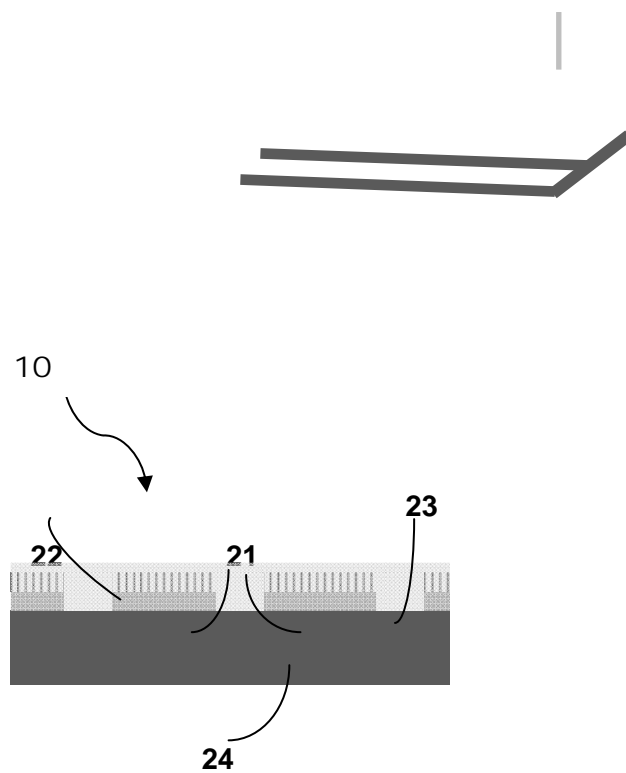
Fig. C-1. Fabrication traveler

Substrate

Metalize top and two edges

Grow vertically oriented graphene

Laser scribe through metalization

Overcoat with electrolyte

Stack and electrically interconnect every 2 cells (alternate opposite faces)

12

20

10

12

11

13

11

12

Fig. C-2A. Prior art

10

22

21

23

24

Fig. C-2B. Cross section of planar EDLC

Width = 6 mm

0.6 inch

20

20 µm

20 µm

200 µm

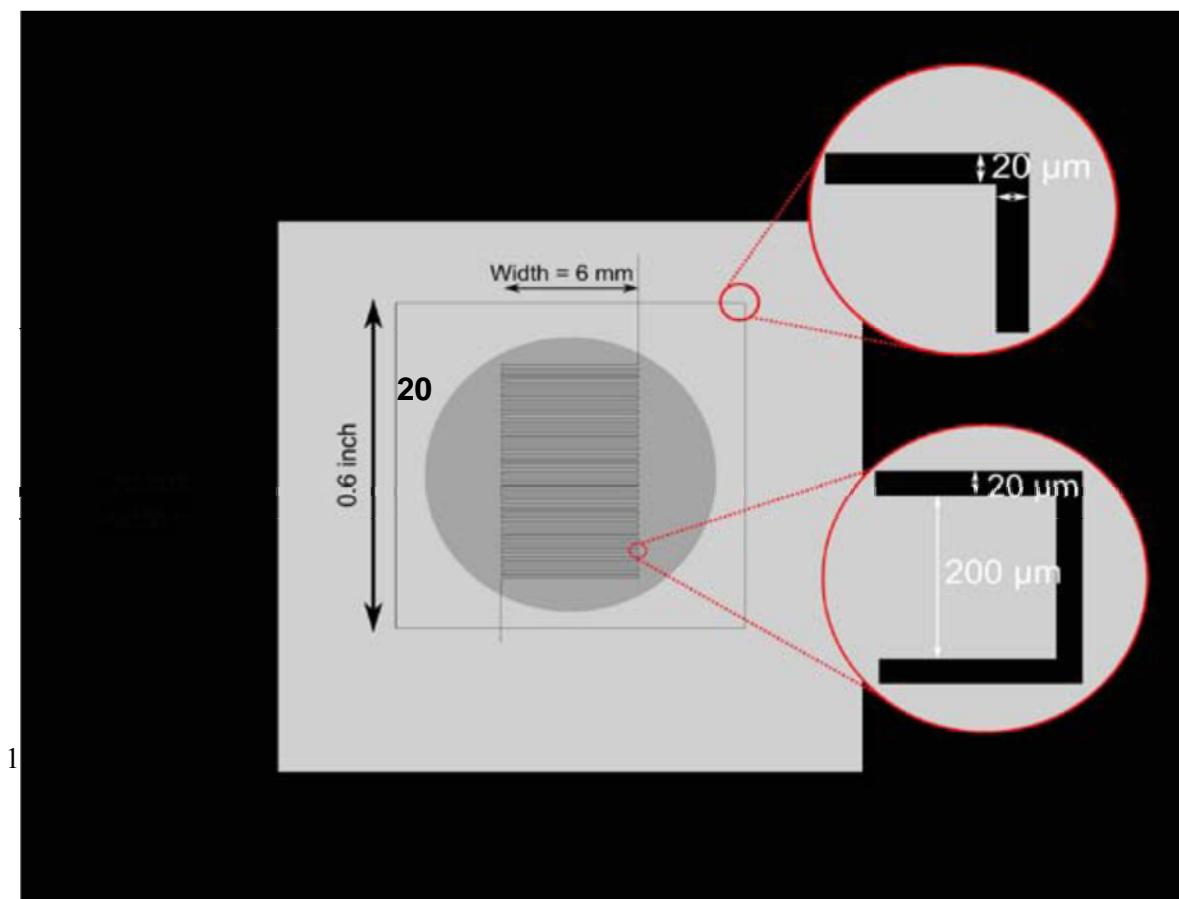**Fig. C-3. Interdigitated square wave gap pattern created by laser ablation**

+   -

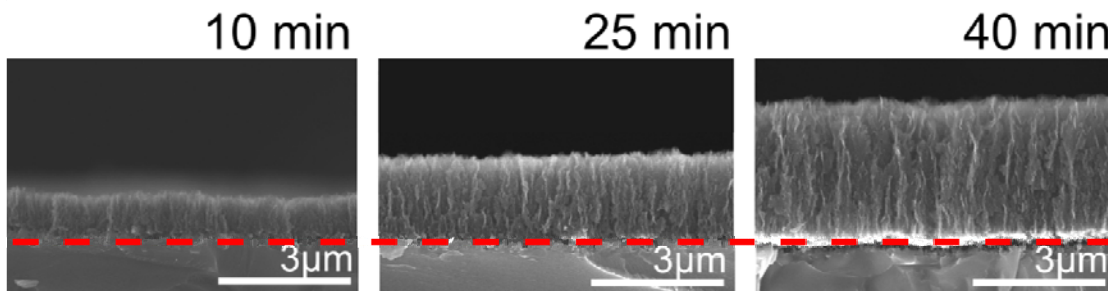**Fig. C-4. Rows of interdigitated square wave gap connected in series (present invention)**

10 min   25 min   40 min

3μm   3μm   3μm

Fig. C-5. Cross section of vertically oriented graphene grown on Ni/Cr/Si film with increasing growth time. Red line is the interface.

Figures C-1 through C-4 show the traveler and schematics of the square wave gap created by laser ablation. A diode-pumped 355nm laser (Tripled YAG) in a direct-write process, using a

10x microspot UV objective was used. Energy out of the laser was ~80μJ at a pulse repetition rate of 60kHz. That beam then was passed through a 770μm aperture to achieve the desired initial spot size (~20μm). The VOG coating was for only 20 minute growth which is a little over 1 μm in thickness (growth rate shown in figure C-5. The capacitive data shown below was based on this coating thickness and a 20 μm gap using PVA/KOH gel electrolyte and a 0.5 volt bias. Gaps approaching 1 μm are possible which substantially increases the capacitance.
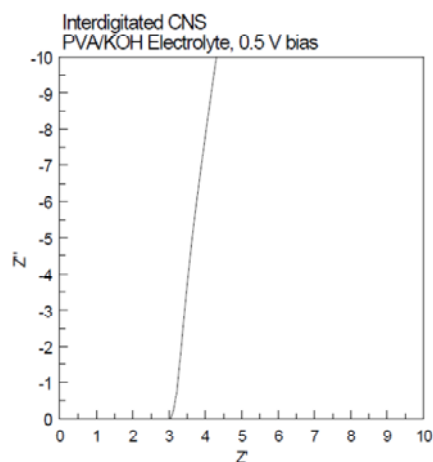

Fig. C-6. Complex plane plot from electrochemical impedance spectroscopy (EIS) results
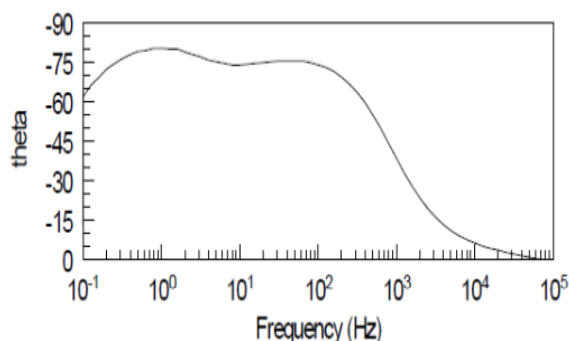

Fig. C-7. Bode representation from EIS. Phase angle in degrees vs frequency

In this initial effort, the results are far from optimal, but show great promise. Figure C-6 is a complex plot obtained from electrochemical impedance spectroscopy (EIS) and shows an equivalent series resistance (ESR) of 3 ohms. For proof of concept, the laser ablation of the gap was run only long enough to achieve a modest resistance of 25 MΩ so this can be significantly improved. In the Bode plot, a phase angle of -75 degrees was achieved at 120 Hz which indicates the use of this design to be quite promising and functional for filtering purposes. Figure C-7 shows useful capacitance even to 10 kHz and a specific capacitance of ~150 μF cm^{-2} .
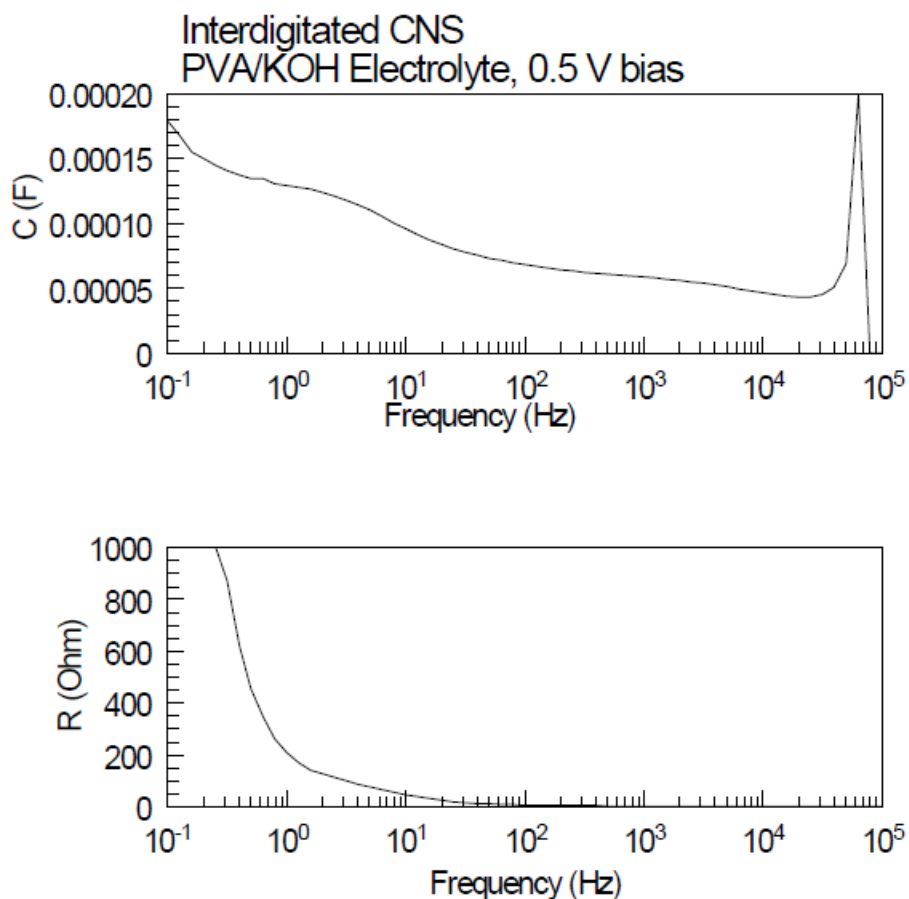
15

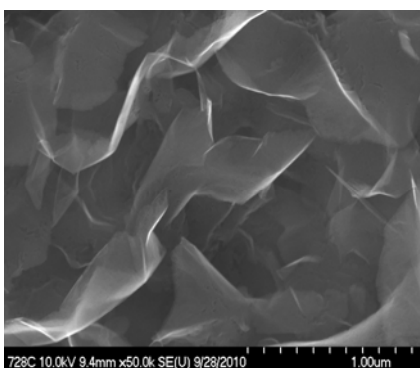Fig. C-8. EIS results. Capacitance and resistance vs frequency

Task D. Parametric study to grow CNS on aluminum substrates.

Although great progress was made on this task, it was not completed because the request for a no cost extension was denied. In order to focus and advance this new EDLC capability to a useful economic end, it is necessary to grow these capacitors on conventional substrates (e.g., Al is frequently used for electrolytic capacitors) such that they can be fabricated into capacitance levels required for military and civilian applications. This requires the utilization of aluminum substrates that can be rolled into useful capacitance levels. The major effort of the growth of CNS to date has been on Ni, Ta and other substrates at temperatures greater than 700°C. The low melting point for Al (660°C) and the low initial emissivity of Al are limitations with CH_4 as feedstock. If, however, a thin, anodized Al surface is the starting substrate (initial high emissivity changes the temperature minimally during growth) and C_2H_2 is used as the feedstock, the set of
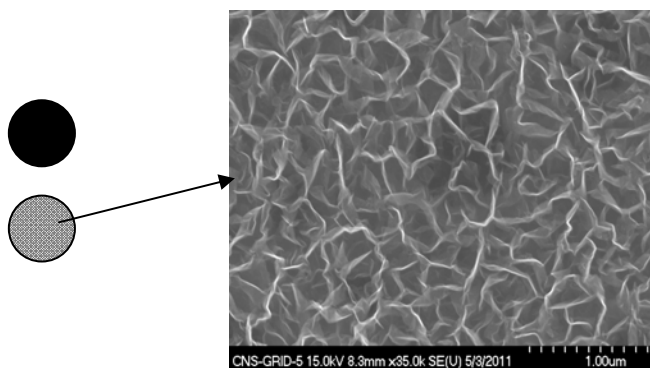
RF PECVD parameters which will allow formation of the CNS can be established. The resistance of the intermediate anodized layer can then be removed by heat treating such that some oxygen will initially evaporate as CO or CO_2 and the balance dissolve into solid solution within the Al bulk. Using acetylene, we have recently grown CNS at temperatures less than 660°C onto Si wafers[17].

The first challenge was to determine a parametric window for the growth of VOG on Al which is quite narrow due to the low melting point (660°C) and the previous parametric set using CH_4 as carbon feedstock and Ni as the substrate. The best growth results obtained to date on Ni require a heater temperature >700ºC. The approach to solve this issue was to change the feedstock from CH_4 to C_2H_2 which allows twice the carbon atoms and ions in the plasma and results in twice the growth rate. Further, a parametric study to adjust all the controlling parameters to lower the growth temperature to below 660ºC was required. In order to achieve the precision necessary to accomplish this task, a number of improvements to the present growth facility were implemented. Replacement of dial type current and voltage indicators with more accurate digital meters was completed. The existing flow controllers, which are a mix of old, un-calibrated instruments from instrument storage that had higher full scale flow ranges (notoriously inaccurate at low flow rates), to new calibrated MKS versions for CH_4, C_2H_2, Ar and H_2 was completed. Also, a system for gas analysis using an SRS 100 mass spectrometer (with separate differential pumping) was added. This will allow direct line of sight assessment of plasma species.

A Langmuir probe for RF plasma was also designed (not yet fabricated). With the mass spectrometer facility, we can determine the density of each ion specie in the plasma so that, along with the Langmuir probe, we have good plasma characterization. A new Alcatel vacuum pump with lower ultimate pressure was also installed to replace the old rotary vane pump. Mechanically polished flat Ta masks were employed in combination with optically flat Al_2O_3 platens to improve the heat transfer over the substrate surface of existing substrate heater. This insured uniform temperature over the metal foil substrate during growth. Although the melting point of Ni is not a concern, a hot spot on an Al substrate is a concern because if any part of the Al melted it would spread over the entire foil immediately, which destroys the film and substrate.

(a)　　　　　　　　　　　　　　　　　　　　　(b)

Figure D-1. Comparison of floating growth (left) which was probably near the plasma potential with the growth at 0V within the W grid (right). Scale bar is 1 μm.

Figure D-1a shows the morphology achieved with the heretofore utilized procedure of allowing the substrate to float with the plasma. Although we have taken most of the previous data with this condition, a simple experiment with grounding the substrate with a single wire resulted in a radial growth around the wire with excellent verticality. This clearly showed that the growth was from ions in the plasma. The transfer of that behavior to uniformly cover a substrate surface was not immediately obvious. Our first attempt in doing this was with a grounded high transmission Ni electroformed grid lying flush against the Ni substrate. One difficulty was insuring that the grid was planar and touched the substrate at every surface point. A second difficulty was having the Ni grid diffusion bond with the substrate. We then went to a stiffer W grid under the mask shown in figure A-1. Figure D-1b shows the substantial improvement in verticality and the substantial increase in density. This became the procedure for all the work presented in this report. At present, we are testing this mode of growth for capacitance properties using a more negative bias to see if further improvement can be obtained. Experiments with negatively biased high transmission W grid mesh sizes of (4 lines per mm and 2 lines per mm) placed on the substrate surface are presently being studied and show a further increase in the sheet density, but electronic problems with the RF, overwhelming the dc power supply, require further electronic refinement (Faraday cage). The plasma in the center of the mesh elements to the substrate surface or to the mesh edge is $\delta \sim 125$ micrometers and the mean free path at 100 mTorr (133 mbar) of the CH_4/H_2 plasma is $\lambda \sim 500$ micrometers. This results in an unimpeded ion trajectory to the substrate and is why the growth predominantly occurs as a result of ion transport (C^+, CH^+, CH_2^+, CH_3^+ and CH_4^+) as opposed to neutrals.
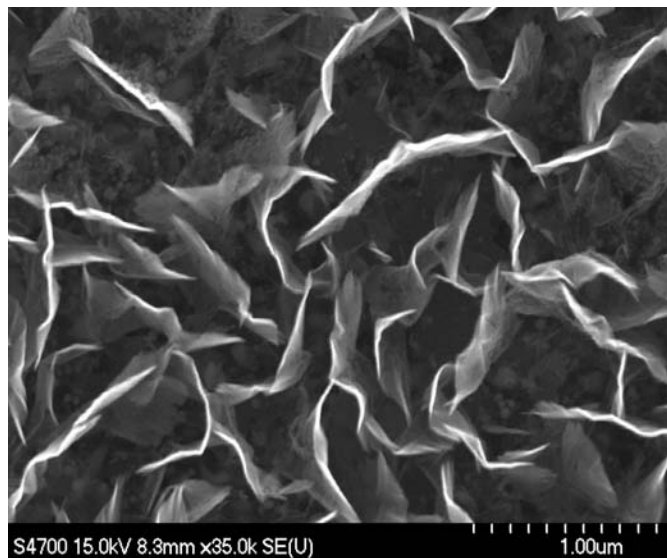

Figure D-2. Plan view of VOG growth morphology on Ni at 600ºC and 0V substrate bias. The scale bar is 1 micrometer.

Following temperature calibration with heater current, the first result of growth using this improved system was recently done with C_2H_2 on a Ni substrate (0V potential and no grid) at low temperature (600ºC). See figure D-2. Although the sheet thicknesses are slightly larger than achieved with CH_4, the films appear to be of excellent morphology with good verticality. This initial work is quite promising and suggests a high probability of success with Al substrates. The high purity (99.999%) polycrystalline Al substrates are in hand and experiments with these foils are imminent, but parametric studies with Ni must first be done to optimize the growth morphology at the lowest temperature possible. This is necessary to reduce the possibility of a catastrophic failure with the Al (melting would destroy the substrate heater). The Ni work is also highly promising and should provide an excellent publishable result.

18

Relevance to the Army

The projected reduction in weight and volume over SOA capacitor elements used in power electronics equipment is greater than a factor of 10. Presently, we have achieved a factor of 6. These savings are applicable to all branches of the military as well as the civilian sector. This translates into substantial reduction in voltage sources for equipment required for each marine and soldier. Furthermore, this advance alters weight and volume constraints for all new military system designs, especially orbital requirements for satellites and payloads. It should also impact the weight and volume of aircraft electronics.

Collaborations and technology transfer

We worked with Professor Steve George in the Chemistry Department at the University of Colorado to use Atomic Layer Deposition to determine the contribution of edge density as compared to the surface area. Professor George was sent 10 pairs of VOG/Ni with plans to coat them with MnOx. He did preliminary work with ALD on Al_2O_3/SiO_2 (glassy) substrates. Growth on VOG is underway.

We have received all Ni foils from Nanotecture in Southampton, England for NiO(OH) coatings on edges of carbon nanosheets to test for improved capacitance, but observed no significant improvement.

Journal publications from this research

J.M. Miller, R.A. Outlaw and B.C. Holloway, "Graphene Electric Double Layer Capacitor with Ultrahigh Power Performance", **Electrochimica Acta** (2010) doi 10.1016/j. electacta 2011.05.122 .

M. Cai, R.A. Outlaw, S.M. Butler and J.M Miller, "A high density of vertically oriented graphenes for EDL supercapacitors", Carbon, 50 (2012) 5481

M. Cai, R.A. Outlaw, S.M. Butler and J.M.Miller: "The Electrolyte Wetting of Vertically Oriented Graphene", Appl. Phys. Lett., in prep.

M. Cai, R.A. Outlaw, S.M. Butler and J.R. Miller, "Ar ion bombarded vertically oriented graphene EDL supercapacitors", Appl. Phys. Lett., in prep.

Graduate students involved during reporting period

- Michael Bagge-Hansen, received his Ph.D. in Applied Science, 15 May 2011.

- Minzhen Cai will complete her Applied Science Ph.D. program in December 2012. She will continue her work in this area as a post doctorate.

Awards, Honors and Appointments

Dr. Bagge-Hansen was awarded the distinction of best science dissertation at the College of William and Mary for 2011.

References

1. Zhao, X., Outlaw, R.A., Wang, J.J., Zhu, M., Smith, G.A. and Holloway, B.C., "Thermal Desorption of Hydrogen from Carbon Nanosheets", J. Chem. Phys. 124 (2006) 194704 .
2. Wang, J et.al.., "Synthesis of carbon nanosheets by inductively coupled radio frequency plasma enhanced chemical vapor deposition", Carbon 42 (2004) 2867-2872.
3. Miller, J.M., Outlaw, R.A. and Holloway, B.C., "Graphene Double Layer Capacitor Capable of Efficient AC Filtering", Science, 329 (2010) 1637.
4. Ferrari, A.C., Robertson, J., "Interpretation of Raman spectra of disordered and amorphous carbon", Phys. Rev. B, 61 2000) 14095.
5. Pimenta, M.A., Dresselhaus, G, Dresselhaus, M.S., Cancado, L.G., Jorio, A., Saito, R., "Studying disorder in graphite based systems by Raman spectroscopy", Phys. Chem. Chem. Phys. 9(2007)1276.
6. Cancado, L.G., Takai, K., Enoki, T., Endo, M., Mizusaki, H., "General equation for the determination of the crystallite size of nanographite by Raman spectroscopy", Appl. Phys. Lett. 88(2006)163106.
7. Zhu, M., Wang, J., Holloway, B.C., Outlaw, R.A., Zhao, X., Hou, K., Shutthanandan, V. and Manos, D.M., "A Mechanism for Carbon Nanosheet Formation", Carbon, 45 (2007) 2229
8. Miller, J.M. , Outlaw, R.A. and Holloway, B.C., "Graphene Double Layer Capacitor with ac Filtering Performance", Electrochimica Acta, 56 (1011)10443
9. Pandolfo, G., Hollenkamp, A.F., "Carbon properties and their role in supercapacitors", J Power Sources;157(2006)11–27.
10. Holloway, P. H.; and Outlaw, R. A.: "The Effect of Temperature Upon NiO Formation and Oxygen Removal on Ni (110)". Surface Science, 12A(1981)1809
11. Frackowiak, E., Béguin, F., "Carbon materials for the electrochemical storage of energy in capacitors". Carbon 39(2001) 937
12. Sheng K, Sun Y, Li C, Yuan W, Shi G. Ultrahigh-rate supercapacitors based on eletrochemically reduced graphene oxide for ac line-filtering. Sci Rep 2012;2:247.

13. Randin, J.P., Yeager, E. "Differential capacitance study of stress annealed pyrolytic graphite electrodes", J Electrochem Soc.;118(1971)711.
14. Randin, J.P, Yeager, E. "Differential capacitance study on the basal plane of stress-annealed pyrolytic graphite". J Electroanal Chem Interfacial Electrochem; 36(1972)257.
15. Kim, T., Lim, S., Kwon, K., Hong, S.H., Qiao, W, Rhee, C.K., et al., "Electrochemical capacitances of well-defined carbon surfaces". Langmuir 22(2006)9086.
16. Cai, M., Outlaw, R.A., Butler, S.M., and Miller, J.M., Carbon (in preparation).
17. Zhu, M., Outlaw, R.A., Bagge-Hansen, M., Chen, H.J. and Manos, D.M., "Field Emission of CNS from C_2H_2 feedstock", Carbon, 49 (2011) 2526